Energy and Enstrophy Spectra of Geostrophic Turbulent Flows Derived from a Maximum Entropy Principle

W. T. M. VERKLEY

Royal Netherlands Meteorological Institute (KNMI), De Bilt, Netherlands

PETER LYNCH

School of Mathematical Sciences, University College Dublin, Belfield, Dublin, Ireland

(Manuscript received 18 July 2008, in final form 29 January 2009)

ABSTRACT

The principle of maximum entropy is used to obtain energy and enstrophy spectra as well as average relative vorticity fields in the context of geostrophic turbulence on a rotating sphere. In the unforced-undamped (inviscid) case, the maximization of entropy is constrained by the constant energy and enstrophy of the system, leading to the familiar results of absolute statistical equilibrium. In the damped (freely decaying) and forced-damped case, the maximization of entropy is constrained by either the decay rates of energy and enstrophy or by the energy and enstrophy in combination with their decay rates. Integrations with a numerical spectral model are used to check the theoretical results for the different cases. Maximizing the entropy, constrained by the energy and enstrophy, gives a good description of the energy and enstrophy spectra in the inviscid case, in accordance with known results. In the freely decaying case, not too long after the damping has set in, good descriptions of the energy and enstrophy spectra are obtained if the entropy is maximized, constrained by the energy and enstrophy in combination with their decay rates. Maximizing the entropy, constrained by the energy and enstrophy in combination with their (zero) decay rates, gives a reasonable description of the spectra in the forced-damped case, although discrepancies remain here.

1. Introduction

The near-two-dimensional nature of large-scale quasigeostrophic (quasi-nondivergent) flow in the atmosphere enables us to study its properties using theories of two-dimensional turbulence (Charney 1971). Two-dimensional incompressible fluid flow is governed by advection of vorticity, implying the conservation of global integrals of any function of the vorticity—in particular of the squared vorticity (enstrophy)—in case the fluid motion is inviscid (i.e., unforced and undamped). Inviscid two-dimensional turbulence is severely constrained by the conservation of enstrophy in addition to energy, as was first demonstrated by Onsager (1949) for a statistical mechanical model based on point vortices. Onsager's contributions, highlighted in a recent review by Eyink and Sreenivasan (2006), initiated a long series of investigations into the problem of two-dimensional turbulence using the techniques of equilibrium statistical mechanics (Kraichnan and Montgomery 1980). Applications of these techniques to the study of turbulent large-scale atmospheric flow, in which the effects of planetary rotation and orography are taken into account, are given by Frederiksen and Sawford (1981), Carnevale and Frederiksen (1987), and Salmon (1998). Equilibrium statistical mechanical theories that incorporate all inviscid invariants of two-dimensional fluid flow—except for invariants of a topological nature (Pasmanter 1994)—are developed by Miller (1990), Miller et al. (1992), and Robert and Sommeria (1991, 1992).

No matter how useful, these theories have to face the criticism that equilibrium statistical mechanics is inapplicable to a dissipative, irreversible process such as turbulence (Eyink and Sreenivasan 2006, p. 99). Other approaches have therefore been developed such as the inertial range theory of Kraichnan (1967) and Batchelor (1969), critically revisited by Dritschel et al. (2007). Thompson (1973) developed an approach based on a randomly forced Liouville equation; this was recently

Corresponding author address: Dr. W. T. M. Verkley, Royal Netherlands Meteorological Institute (KNMI), P.O. Box 201, 3730 AE De Bilt, Netherlands.
E-mail: verkley@knmi.nl

DOI: 10.1175/2009JAS2889.1

© 2009 American Meteorological Society

extended to a spherical geometry by Kurgansky (2008). As a somewhat unorthodox application of the techniques of statistical mechanics, Burgers (1939) also developed a theory of forced-dissipative turbulence. Rather different from the approach that Onsager (1949) was to adopt later, Burgers divided the phase space of a spectrally truncated fluid system into discrete cells and described the system statistically by associating frequencies with the different cells. Following usual practice, he then searched for the frequency distribution with the highest multiplicity (i.e., that can be realized microscopically in the largest number of ways), using the constraint—and this was unusual—that forcing and dissipation of energy should balance on average. The result of his analysis is equipartition of dissipation instead of equipartition of energy. [See also Burgers (1974), Nieuwstadt and Steketee (1995), and, for readers familiar with Dutch, Burgers (1941).] In this article we wish to build further on Burgers' approach to forced-dissipative turbulence.

If we identify a frequency distribution with a probability density function, then maximizing its multiplicity is, for all practical purposes, equivalent to maximizing Shannon's information entropy. Frequency distributions with the highest multiplicity can be realized by nature in the largest number of ways so that probability density functions with maximum entropy are optimal statistical descriptions of any system. This underlies the principle of maximum entropy that has been advocated by Jaynes in two papers on statistical physics (Jaynes 1957a,b). It states that the preferred probability density function of any system is the one that maximizes the information entropy, constrained by the normalization condition and the available information. The latter is usually assumed to be in the form of averages of the quantities of interest. In several publications (see Rosenkrantz 1989), Jaynes has shown that the principle of maximum entropy can be applied to many problems for which we have incomplete information, ranging from the description of a classical ideal gas to the correction of images.[1]

We will apply the principle of maximum entropy to study the statistics of the equivalent barotropic vorticity equation on a rotating sphere. This equation was used by Ambaum (1997) to study the dynamics of the tropopause and can be considered as a first-order model of the general circulation of the atmosphere. The model is closely analogous to the model that was studied by Frederiksen and Sawford (1981) and Carnevale and Frederiksen (1987) and, more recently, by Majda and Wang (2006). In studying the statistical mechanics of this model we effectively take up Burgers' thread again by using energy and enstrophy, as well as their decay rates, as relevant information in the description of forced-dissipative turbulence. We will start by studying the unforced-undamped case to verify results known from the literature, but we concentrate on the freely decaying and the forced-damped case. Our focus will be on the energy and enstrophy spectra and averages of the relative vorticity field that can be calculated from the probability density functions.

In section 2, we set up the framework of constrained entropy maximization, deduce the resulting probability density function, and derive general expressions for the mean and variance of the system components. The equivalent barotropic vorticity equation is introduced in section 3. In section 4 we apply the general formulas obtained in section 2 to the unforced-undamped case. Here the entropy is maximized, keeping the energy and enstrophy of the system fixed. We check the results against a long numerical run with the unforced-undamped model. We then, in section 5, apply the general results of section 2 to the case in which both forcing and damping are present. First, the entropy is maximized with the decay rates of energy and enstrophy as constraints. Although the procedure is closely analogous to the procedure in the unforced-undamped case, the results are quite different. We then give the basic expressions in the case where the entropy is maximized, keeping both the energy and enstrophy as well as their decay rates constant.

Two further numerical runs are studied to check the results. The first is an ensemble of 100 integrations, with damping in the form of Newtonian viscosity, starting from 100 different initial states at the end of the previous unforced-undamped integration. The second is a long run with the forced-damped version of the model, spun up from the state of rest. We demonstrate that the combination of energy and enstrophy and their decay rates in the maximization of entropy gives a good description of the spectra and numerical averages in the freely decaying case, not too long after the dissipation has set in. In the forced-damped case we show that the spectra and theoretical averages based on the (zero) decay rates of energy and enstrophy are better descriptions of the numerical results than the corresponding spectra and theoretical averages based on values of the energy and enstrophy that are taken from the numerical run. The use of both the (zero) decay rates of energy and enstrophy as well as the values of energy and enstrophy themselves (taken from the numerical run) improves the resemblance between theory and numerical simulations, although discrepancies still remain. In section 6 we give our conclusions and discuss possible extensions of the present approach.

[1] All of Jaynes' papers, published and unpublished, can be downloaded from http://bayes.wustl.edu/etj/node1.html.

2. Entropy maximization

Quite generally, we assume that the state of the physical system under investigation can be specified by means of a state vector $\mathbf{x} = (x_1, x_2, \ldots, x_M)$, where M is the number of degrees of freedom. We introduce a probability density function (or distribution function) $\mathcal{P}$ for the occurrence of this state:

$$\mathcal{P} = \mathcal{P}(\mathbf{x}) = \mathcal{P}(x_1, x_2, \ldots, x_M). \tag{1}$$

Our objective is to find an expression for $\mathcal{P}$ in terms of the state vector $\mathbf{x}$. The principle of maximum entropy requires that the probability density function $\mathcal{P}$ should be as broad as possible, given the available information on the system. The degree of broadness is measured by the following continuous extension of Shannon's information entropy (see Jaynes 1968):

$$\mathcal{S}_I = -\int \mathcal{P}(\mathbf{x}) \log \frac{\mathcal{P}(\mathbf{x})}{\mathcal{M}(\mathbf{x})}\, dx = -\int \cdots \int \mathcal{P}(x_1, x_2, \ldots, x_M) \log \frac{\mathcal{P}(x_1, x_2, \ldots, x_M)}{\mathcal{M}(x_1, x_2, \ldots, x_M)}\, dx_1\, dx_2 \cdots dx_M, \tag{2}$$

where $dx = dx_1 dx_2 \cdots dx_M$ and the integration is over all values of $x_1, x_2, \ldots, x_M$. The definition of the entropy $\mathcal{S}_I$ involves a measure $\mathcal{M}$,

$$\mathcal{M} = \mathcal{M}(\mathbf{x}) = \mathcal{M}(x_1, x_2, \ldots, x_M), \tag{3}$$

which is the probability density function that represents our knowledge of the system given only background information (e.g., on the physical nature of the coordinates $x_1, x_2, \ldots, x_M$). Choosing this measure is not straightforward, but guidelines, based on group invariance arguments, can be found in Jaynes (1968, 1973). Here we make the following simple choice:

$$\mathcal{M}(x_1, x_2, \ldots, x_M) = c_1^{-1} c_2^{-1} \cdots c_M^{-1} = \prod_m c_m^{-1}, \tag{4}$$

where c_m are constants having the same dimension as the coordinates x_m. When the range of coordinates is infinite, as in our case, this probability density function is not normalizable. In practice, however, it is the normalizability of $\mathcal{P}$ that is required, so this is no cause of concern.

Once we have made a choice of $\mathcal{M}$ in a particular set of coordinates, the expression (2) of the entropy $\mathcal{S}_I$ is invariant for a transformation to another set of coordinates.[2] To show this, let these other coordinates be denoted by $\mathbf{y} = (y_1, y_2, \ldots, y_M)$. Marking by primes the probability density functions in the transformed coordinates, we have

$$\mathcal{P}(\mathbf{x})\, dx = \mathcal{P}'(\mathbf{y}) dy \quad \text{and} \tag{5}$$

$$\mathcal{M}(\mathbf{x})\, dx = \mathcal{M}'(\mathbf{y}) dy. \tag{6}$$

This implies

$$\frac{\mathcal{P}(\mathbf{x})}{\mathcal{M}(\mathbf{x})} = \frac{\mathcal{P}'(\mathbf{y})}{\mathcal{M}'(\mathbf{y})}, \tag{7}$$

so that

$$\int \mathcal{P}(\mathbf{x}) \log \frac{\mathcal{P}(\mathbf{x})}{\mathcal{M}(\mathbf{x})} dx = \int \mathcal{P}'(\mathbf{y}) \log \frac{\mathcal{P}'(\mathbf{y})}{\mathcal{M}'(\mathbf{y})}\, dy, \tag{8}$$

from which the invariance of $\mathcal{S}_I$ immediately follows. It should be realized, however, that $\mathcal{S}_I$ is not invariant under a change of the measure $\mathcal{M}$. For example, if the values d_m instead of c_m are chosen in (4), the entropy changes by an amount $\Sigma_m \log(c_m/d_m)$.

In maximizing the entropy $\mathcal{S}_I$ the probability density function $\mathcal{P}$ is constrained by the normalization condition:

$$\int \mathcal{P}(\mathbf{x}) dx = 1. \tag{9}$$

In addition, we consider constraints on some function or functions $\mathcal{K}_\ell(\mathbf{x})$, assuming that their expected values are given:

$$\int \mathcal{P}(\mathbf{x}) \mathcal{K}_\ell(\mathbf{x}) dx = \mathcal{K}_\ell^0 \quad \ell = 1, 2, \ldots, L, \tag{10}$$

where $\mathcal{K}_\ell^0$ are specified numbers. The requirement that $\mathcal{S}_I$ be maximal, subject to the constraints above, leads to the following condition:

$$\int \delta\mathcal{P}(\mathbf{x}) \left[\log \frac{\mathcal{P}(\mathbf{x})}{\mathcal{M}(\mathbf{x})} + 1 + \rho + \sum_\ell \lambda_\ell \mathcal{K}_\ell(\mathbf{x}) \right] dx = 0, \tag{11}$$

where ρ and λ_ℓ are the Lagrange multipliers associated with the constraints (9) and (10), respectively. At a maximum of $\mathcal{S}_I$ this condition should hold for arbitrary variations $\delta\mathcal{P}$, so that the quantity between parentheses has to be zero. This leads to the following expression of the probability density function:

$$\mathcal{P}(\mathbf{x}) = \frac{1}{\mathcal{Z}} \mathcal{M}(\mathbf{x}) \exp\left[-\sum_\ell \lambda_\ell \mathcal{K}_\ell(\mathbf{x}) \right]. \tag{12}$$

The quantity $\mathcal{Z} = \exp(\rho + 1)$ is determined from the normalization constraint (9) and will depend on the

[2] Such a set of coordinates could be the result of a deterministic time-evolution, implying that the entropy $\mathcal{S}_I$ would—in that case—be independent of time.

Lagrange multipliers λ_ℓ. It is called the partition function ($\mathcal{Z}$ stands for *Zustandsumme* or sum over states):

$$\mathcal{Z} = \mathcal{Z}(\lambda_\ell) = \int \mathcal{M}(\mathbf{x}) \exp\left[-\sum_\ell \lambda_\ell \mathcal{K}_\ell(\mathbf{x})\right] dx. \tag{13}$$

The probability density function $\mathcal{P}$ in the form of expressions (12) and (13) depends only on the Lagrange multipliers λ_ℓ. These are to be determined from the constraints (10).

Choosing the measure $\mathcal{M}$ as in (4) and limiting ourselves to constraints for which the functions $\mathcal{K}_\ell$ are of the type

$$\mathcal{K}_\ell(x_1, x_2, \ldots, x_M) = \sum_m (A_{\ell m} x_m^2 + B_{\ell m} x_m + C_{\ell m}), \tag{14}$$

the probability density function may be written

$$\mathcal{P}(x_1, x_2, \ldots, x_M) = \frac{1}{\mathcal{Z}} \prod_m c_m^{-1} \exp\left\{-\left[\left(\sum_\ell \lambda_\ell A_{\ell m}\right) x_m^2 + \left(\sum_\ell \lambda_\ell B_{\ell m}\right) x_m + \left(\sum_\ell \lambda_\ell C_{\ell m}\right)\right]\right\}. \tag{15}$$

The expression in braces can be put into the form

$$-\frac{1}{2\sigma_m^2}[(x_m - \mu_m)^2 + \tau_m - \mu_m^2], \tag{16}$$

where

$$\sigma_m^2 = \frac{1}{2\sum_\ell \lambda_\ell A_{\ell m}}, \quad \mu_m = -\frac{\sum_\ell \lambda_\ell B_{\ell m}}{2\sum_\ell \lambda_\ell A_{\ell m}}, \quad \tau_m = \frac{\sum_\ell \lambda_\ell C_{\ell m}}{\sum_\ell \lambda_\ell A_{\ell m}}. \tag{17}$$

This means that the probability density function can be written as

$$\mathcal{P}(x_1, x_2, \ldots, x_M) = \frac{1}{\mathcal{Z}} \prod_m c_m^{-1} \exp\left(\frac{\mu_m^2 - \tau_m}{2\sigma_m^2}\right) \sigma_m \sqrt{2\pi} \times \mathcal{N}(\mu_m, \sigma_m, x_m), \tag{18}$$

where $\mathcal{N}$ is the normal distribution, given by

$$\mathcal{N}(\mu, \sigma, x) = \frac{1}{\sigma\sqrt{2\pi}} \exp\left[-\frac{(x-\mu)^2}{2\sigma^2}\right]. \tag{19}$$

The normal distribution has the following properties:

$$\int \mathcal{N}(\mu, \sigma, x) dx = 1, \quad \int \mathcal{N}(\mu, \sigma, x) x\, dx = \mu, \quad \text{and} \quad \int \mathcal{N}(\mu, \sigma, x) x^2 dx = \sigma^2 + \mu^2. \tag{20}$$

The first of these properties can be used to obtain the partition function $\mathcal{Z}$ by applying the normalization condition to $\mathcal{P}$:

$$\mathcal{Z} = \prod_m c_m^{-1} \exp\left(\frac{\mu_m^2 - \tau_m}{2\sigma_m^2}\right) \sigma_m \sqrt{2\pi}. \tag{21}$$

For the probability density function $\mathcal{P}$ we thus have

$$\mathcal{P}(x_1, x_2, \ldots, x_M) = \prod_m \mathcal{N}(\mu_m, \sigma_m, x_m), \tag{22}$$

which is a product of M normal distributions in the different variables. The variables are uncorrelated and each component has its own mean μ_m and variance σ_m. The probability density function $\mathcal{P}$ is fully determined by the constraints (10) and is independent of the values c_m chosen in the measure $\mathcal{M}$.

The parameters μ_m and σ_m, which determine the form of the probability density function, depend on the Lagrange multipliers λ_ℓ as expressed by (17). The Lagrange multipliers, in turn, are determined by the expected values of the functions $\mathcal{K}_\ell^0$. Using angle brackets to denote the expectation operator,

$$\langle \mathcal{K} \rangle = \int \mathcal{P}(\mathbf{x}) \mathcal{K}(\mathbf{x}) dx = \int \cdots \int \mathcal{P}(x_1, x_2, \ldots, x_M) \mathcal{K}(x_1, x_2, \ldots, x_M)\, dx_1 dx_2 \cdots dx_M, \tag{23}$$

the constraints [(10)] can be written as

$$\langle \mathcal{K}_\ell \rangle = \mathcal{K}_\ell^0 \quad \ell = 1, 2, \ldots, L. \tag{24}$$

Because the expectation operator is linear, we have

$$\langle \mathcal{K}_\ell \rangle = \sum_m (A_{\ell m} \langle x_m^2 \rangle + B_{\ell m} \langle x_m \rangle + C_{\ell m}). \tag{25}$$

For any function $f(x_m)$ that depends only on a single component x_m, we can write

$$\begin{aligned}\langle f\rangle &= \int\cdots\int\prod_k \mathcal{N}(\mu_k,\sigma_k,x_k)f(x_m)\,dx_1\,dx_2\cdots dx_M\\ &= \left[\prod_{k\neq m}\int\mathcal{N}(\mu_k,\sigma_k,x_k)\,dx_k\right]\int\mathcal{N}(\mu_m,\sigma_m,x_m)f(x_m)dx_m\\ &= \int\mathcal{N}(\mu_m,\sigma_m,x_m)f(x_m)dx_m,\end{aligned}\tag{26}$$

where we have again used the first of the properties of $\mathcal{N}$ in (20). Using the second and third of these properties and the expression just derived, we find that

$$\langle x_m\rangle = \mu_m,\quad \langle x_m^2\rangle = \sigma_m^2+\mu_m^2.\tag{27}$$

Substituting this in (25), we get

$$\langle\mathcal{K}_\ell\rangle = \sum_m\left[A_{\ell m}(\sigma_m^2+\mu_m^2)+B_{\ell m}\mu_m+C_{\ell m}\right].\tag{28}$$

Equating this expression to $\mathcal{K}_\ell^0$ for each ℓ gives us a set of (possibly nonlinear) equations, from which the Lagrange multipliers λ_ℓ can be obtained.

Having found the probability density function (22) that maximizes the entropy $\mathcal{S}_I$, the value of the maximum entropy, denoted by $\mathcal{S}_M$, can be calculated. This value is readily obtained from (2) and (22) and is given by

$$\mathcal{S}_M = \frac{1}{2}\sum_m\log\left[(2\pi e)\frac{\sigma_m^2}{c_m^2}\right].\tag{29}$$

This expression illustrates the notion of the information entropy of a probability density function as a measure of broadness. Indeed, the broader the individual normal distributions are (as measured by their variance σ_m), the larger the entropy $\mathcal{S}_M$ will be. We recall that although the maximum entropy (29) depends on the values of c_m, the corresponding probability density function (22)—which incorporates the information contained in the constraints—is independent of c_m.

3. Equivalent barotropic vorticity equation

In this section we will introduce the system to which the results obtained in the previous section will be applied: a quasigeostrophic model of the general circulation of the atmosphere, called the equivalent barotropic vorticity equation. To establish a geophysical context, we use Ω^{-1} as a unit of time and a as a unit of length, where $\Omega = 7.292\times10^{-5}\ \mathrm{s}^{-1}$ is the earth's rotation rate and $a = 6.371\times10^6$ m is the earth's radius. This gives a velocity unit of $\Omega a = 464.573\ \mathrm{m\ s}^{-1}$. We denote by the number $D = 6.300\,288 \approx 2\pi$ the time corresponding to one (solar) day of 86 400 s, expressed in terms of the time unit Ω^{-1}. Subsequently, we will use days, hours, and minutes to express time (which, by using the value of D, can be expressed straightforwardly in units of Ω^{-1}).

The equivalent barotropic vorticity equation describes the quasigeostrophic (or quasi-nondivergent) dynamics of a shallow layer of fluid:

$$\frac{\partial q}{\partial t}+\mathbf{v}\cdot\nabla q = F+\sum_p(-1)^{p+1}\nu_p\nabla^{2p+2}\psi,\tag{30}$$

where

$$q = f+\zeta-\Lambda\psi+f\frac{\eta_B}{H_A}.\tag{31}$$

Here q is the quasigeostrophic potential vorticity, given by the sum of the planetary vorticity f, the relative vorticity ζ, a stretching (Cressman) term $-\Lambda\psi$, and a contribution $f(\eta_B/H_A)$ due to the orography η_B. The horizontal velocity field $\mathbf{v}$ of the fluid is independent of height and assumed to be nondivergent, enabling us to write $\mathbf{v} = \mathbf{k}\times\nabla\psi$ and $\zeta = \nabla^2\psi$, where ψ is the streamfunction. The flow domain is a rotating sphere on which horizontal positions are denoted by the longitude λ and the latitude ϕ. In the units given above, the Coriolis parameter (or planetary vorticity) is given by $f = 2\sin\phi$. For the stretching parameter $\Lambda = 1/L_R^2$, where L_R is the Rossby radius of deformation, we have (in the same units)

$$\Lambda = \frac{4\Omega^2a^2}{gH_A}\sin^2\phi_0,\tag{32}$$

where H_A is the average height of the fluid, g is the (reduced) acceleration due to gravity, and ϕ_0 is a fixed value of the latitude. The unforced-undamped version of the system (30) and (31) is a simplification of the global equivalent barotropic vorticity equation that was proposed recently by Verkley (2009) and Schubert et al. (2009). In the former reference it is argued that if the simplified system used here is to reproduce asymptotically the phase velocities of Rossby waves in the limit of small meridional wavelengths, we should take $\phi_0 = \pm\pi/4$, implying that $\sin^2\phi_0 = \frac{1}{2}$. We will discuss both the unforced-undamped and the forced-damped version of the system. In the latter case, the forcing is given by F and the damping consists of a sum of various orders of (hyper)viscosity. Without the stretching term [the limit in which the (reduced) gravity approaches infinity] the forced-damped system above is discussed extensively in chapter 16 of Majda and Wang (2006).

Expressing the velocity field in terms of the streamfunction ψ, we may write for the advection term

$$\mathbf{v}\cdot\nabla q=\mathbf{k}\times\nabla\psi\cdot\nabla q=\mathbf{k}\cdot\nabla\psi\times\nabla q=J(\psi,q),\quad(33)$$

where J is the Jacobi operator. This particular form of advection leads to the following global conservation laws for energy E and potential enstrophy[3] Z:

$$\frac{dE}{dt}=\mathcal{F}-\mathcal{D},\quad\text{and}\quad(34a)$$

$$\frac{dZ}{dt}=\mathcal{G}-\mathcal{H},\quad(34b)$$

where

$$\begin{aligned}E&=\frac{1}{4\pi}\int\frac{1}{2}(\mathbf{v}^2+\Lambda\psi^2)dS,\\ \mathcal{F}&=-\frac{1}{4\pi}\int\psi F\,dS,\\ \mathcal{D}&=\frac{1}{4\pi}\int\psi\left[\sum_p(-1)^{p+1}\nu_p\nabla^{2p+2}\psi\right]dS,\\ Z&=\frac{1}{4\pi}\int\frac{1}{2}q^2\,dS,\\ \mathcal{G}&=\frac{1}{4\pi}\int qF\,dS,\quad\text{and}\\ \mathcal{H}&=-\frac{1}{4\pi}\int q\left[\sum_p(-1)^{p+1}\nu_p\nabla^{2p+2}\psi\right]dS,\end{aligned}\quad(35)$$

and all integrals are to be taken over the area of the unit sphere with $dS=\cos\phi d\lambda d\phi$. The expressions of E and Z give the nondimensional energy and enstrophy per unit of nondimensional area. To obtain an indication of the dimensional value of, for example, the total energy, one needs to multiply the corresponding expression by $A=\rho H_A 4\pi a^2(\Omega a)^2$. The factor ρH_A, where ρ is the constant density of the fluid, should correspond to the average total mass of the atmosphere per unit area. This is given by p_s/g, where p_s is the average surface pressure and g is (full) acceleration due to gravity. Using the values 1000 hPa and 9.806 m s^{-2} for these quantities, we obtain $A=1.123\times10^{24}$ J. Because the total (kinetic plus available potential) energy in the atmospheric general circulation is 2.867×10^{21} J [deduced from Fig. 14.8 of Peixoto and Oort (1992)] the value of the nondimensional energy E should be of the order 2.5×10^{-3} if it is to represent a realistic atmospheric value.

It is natural to expand scalar functions on the sphere in terms of spherical harmonics $Y_{mn}(\lambda,\phi)$, $n=0,1,2,\ldots,m=-n,1-n,\ldots,n-1,n$, that we define as follows:

$$Y_{mn}(\lambda,\phi)=\begin{cases}\sqrt{2}R_n^{|m|}(\sin\phi)\cos(|m|\lambda) & \text{for}\quad m>0,\\ R_n^0(\sin\phi) & \text{for}\quad m=0,\\ \sqrt{2}R_n^{|m|}(\sin\phi)\sin(|m|\lambda) & \text{for}\quad m<0,\end{cases}\quad(36)$$

where $R_n^m(x)$ $(-1<x<1)$ is given by

$$R_n^m(x)=(-1)^m\sqrt{(2n+1)\frac{(n-m)!}{(n+m)!}}P_n^m(x)\quad(37)$$

and $P_n^m(x)$ are the associated Legendre functions as given in Abramowitz and Stegun (1970). The spherical harmonics are eigenfunctions of the spherical Laplace operator:

$$\nabla^2Y_{mn}=-e_nY_{mn},\quad(38)$$

where $e_n=n(n+1)$. The functions form an orthonormal set:

$$\frac{1}{4\pi}\int Y_{mn}(\lambda,\phi)Y_{k\ell}(\lambda,\phi)dS=\delta_{mk}\delta_{n\ell}.\quad(39)$$

The expansion coefficients of any field, for example, the relative vorticity field ζ,

$$\zeta(\lambda,\phi,t)=\sum_{mn}\zeta_{mn}(t)Y_{mn}(\lambda,\phi),\quad(40)$$

are therefore given by

$$\zeta_{mn}(t)=\frac{1}{4\pi}\int Y_{mn}(\lambda,\phi)\zeta(\lambda,\phi,t)dS.\quad(41)$$

Because the spherical harmonics Y_{mn} are eigenfunctions of the Laplace operator ∇^2 with eigenvalue $-e_n$, the coefficients of ζ are related to the coefficients of ψ by

$$\zeta_{mn}=-e_n\psi_{mn}.\quad(42)$$

If the field $f+f(h/H)$ is written as

$$f+f\frac{h}{H}=\sum_{mn}f_{mn}Y_{mn},\quad(43)$$

we may write the coefficients of q in terms of the coefficients of ψ:

$$q_{mn}=f_{mn}-\varepsilon_n\psi_{mn},\quad(44)$$

where $\varepsilon_n=\Lambda+e_n$. Note that $\varepsilon_n=O(n^2)$ for large n. Finally, the forcing plus damping term may be written as

$$\sum_{mn}(F_{mn}+d_n\psi_{mn})Y_{mn},\quad(45)$$

[3] From now on we will skip, for convenience, the adjective "potential."

where F_{mn} are the spectral coefficients of the forcing F and where

$$d_n = \sum_p \nu_p e_n^{p+1}. \tag{46}$$

With these definitions we may express E, Z, etc. in terms of the coefficients ψ_{mn} of the streamfunction ψ:

$$\begin{aligned}
E &= \sum_{mn} \frac{1}{2}\varepsilon_n \psi_{mn}^2,\\
\mathcal{F} &= \sum_{mn} -F_{mn}\psi_{mn},\\
\mathcal{D} &= \sum_{mn} d_n \psi_{mn}^2,\\
Z &= \sum_{mn} \left(\frac{1}{2}\varepsilon_n^2 \psi_{mn}^2 - \varepsilon_n f_{mn}\psi_{mn} + \frac{1}{2} f_{mn}^2\right),\\
\mathcal{G} &= \sum_{mn} (-\varepsilon_n F_{mn}\psi_{mn} + f_{mn}F_{mn}), \quad \text{and}\\
\mathcal{H} &= \sum_{mn} (d_n \varepsilon_n \psi_{mn}^2 - d_n f_{mn}\psi_{mn}).
\end{aligned} \tag{47}$$

The evolution equations for the coefficients ψ_{mn} can be written as

$$-\varepsilon_n \frac{d\psi_{mn}}{dt} + \frac{1}{4\pi}\int Y_{mn} J(\psi, q) dS = F_{mn} + d_n \psi_{mn}. \tag{48}$$

Expanding the fields ψ and q in the Jacobian in terms of spherical harmonics, these equations assume the form

$$-\varepsilon_n \frac{d\psi_{mn}}{dt} + \sum_{ij}\sum_{kl} \psi_{ij}(f_{kl} - \varepsilon_k \psi_{kl}) I_{mnijkl} = F_{mn} + d_n \psi_{mn}, \tag{49}$$

where the interaction coefficients I_{mnijkl} are given by

$$I_{mnijkl} = \frac{1}{4\pi}\int Y_{mn} J(Y_{ij}, Y_{kl}) dS. \tag{50}$$

A finite dimensional (spectrally truncated) model is obtained by letting n run from 0 to N and m from $-n$ to $+n$, with N being a finite number, referred to as a triangular truncation TN, and the same for the indices i, j and k, l in the summations of (49). The global energy and enstrophy equations [(34a) and (34b)], after replacing (35) by (47), remain valid for such a finite-dimensional version of the equations, as can be deduced from the symmetry properties of the interaction coefficients. We furthermore note that all quantities involved fit into the general form (14), thus allowing us to apply the principle of maximum entropy for any combination of these quantities as constraints, using the general expressions derived in the previous section.

The model that we will use to check the predictions of the maximum entropy principle is the spectral numerical model in the form of (48). The projection integrals of the Jacobian onto the spherical harmonics Y_{mn} are carried out numerically by summations over a Gaussian grid, equidistant in longitude and Gaussian in the sine of the latitude. The integrals can be calculated exactly if the grid resolution is larger than some minimum resolution that depends on the truncation limit N of the model. More specifically, if the Gaussian grid has $K \times L$ points then the numerical projections are exact if $K \geq 3N - 1$ and $L \geq (3N - 1)/2$. This can be verified by consulting Machenhauer (1979), whose review paper on the spectral method was closely followed in the construction of the model. For our experiments we use a model with truncation $T42$. A Gaussian grid of 128×64 points is then sufficiently dense to perform the projections without approximation. For the time stepping we use a fourth-order Runge–Kutta scheme with a time step of 15 min (0.065807 in units of Ω^{-1}).

In all variants that we will discuss in the following, the right-hand side of (30) is specialized to

$$\begin{aligned}
F + \sum_p (-1)^{p+1} \nu_p \nabla^{2p+2}\psi \\
= \nu_{-1}(\psi - \psi_f) + (-1)^{r+1}\nu_r \nabla^{2r+2}\psi,
\end{aligned} \tag{51}$$

with the understanding that in the unforced-undamped case, all terms on the right-hand side are zero. The forcing is therefore given by $F = -\nu_{-1}\psi_f$, whereas the damping is the sum of a hypoviscosity (longwave damping) term $\nu_{-1}\psi$ and a (hyper)viscosity term $(-1)^{r+1}\nu_r \nabla^{2r+2}\psi$. The values of ν_{-1} and ν_r are written as

$$\nu_{-1} = \frac{\Lambda}{D\tau_{-1}}, \quad \nu_r = \frac{1}{D\tau_r}\frac{1}{e_N^r}, \tag{52}$$

where τ_{-1} and τ_r are expressed in days (recall that we defined $D = 6.300\,288 \approx 2\pi$ to be the nondimensional length of a day). The expression for ν_r implies that the coefficients ζ_{mn} with $n = N$ of the relative vorticity field decay in time according to $\exp(-t/\tau_r)$, where t is expressed in days, neglecting Λ and the nonlinear advection. We take $\tau_{-1} = 90$ days and $\tau_r = 5$ days, with $r = 1$ (viscosity), giving $\nu_{-1} = 1.764 \times 10^{-1}$ and $\nu_r = 1.758 \times 10^{-5}$ nondimensionally. For the scale height H_A we take 10 km whereas for Λ we choose the value 100. These values are consistent with (32) if we take the value 0.432 for the (reduced) acceleration due to gravity.

For the field η_B we choose the earth's orography in T41 truncation, obtained from the European Centre for Medium-Range Weather Forecasts (ECMWF). The field $f(\eta_B/H_A)$ can then be represented exactly in the

T42 truncation of the model. The field ψ_f that we will use in the forced-damped case is the streamfunction that corresponds to two sharply defined (westerly) zonal jet streams, each one having the form

$$u_f(\phi) = U \exp[-(\phi - \phi_0)^2/2\Delta\phi^2], \qquad (53)$$

where $U = 0.050$ and $\Delta\phi = 0.079$. The jet streams are placed at $\phi_0 = \pm\pi/4$ and have velocity maxima of 23.228 m s^{-1}. The spectral coefficients of ψ_f are calculated by evaluating the corresponding relative vorticity field on the Gaussian grid of the model, transforming to spectral space and then applying the inverse Laplace operator. In Fig. 1a we show the field $f(\eta_B/H_A)$ and in Fig. 1b, the streamfunction ψ_f. The profile to the right of Fig. 1b shows the zonal velocity (in m s^{-1}) associated with the streamfunction ψ_f. In the first case considered below, we put forcing and damping to zero but keep the terms $-\Lambda\psi$ and $f(\eta_B/H_A)$ in the expression of the potential vorticity q.

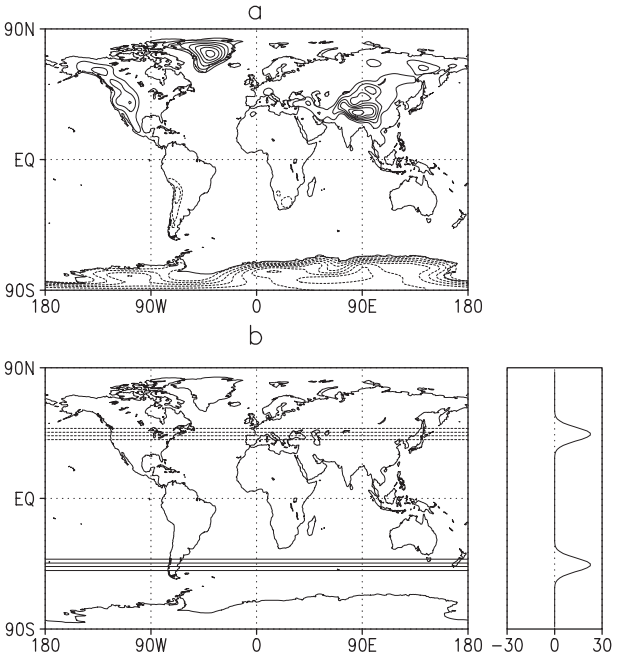

FIG. 1. (a) The scaled orography $f(\eta_B/H_A)$ and (b) the forcing field ψ_f in the T42 truncation of the spectral model. The contour interval in (a) is 0.1 and in (b) is 0.002; negative values are dashed. The zero contour is left out in both panels. The fields in this and similar plots are based on 256 × 128 data points. The profile on the right in (b) shows the zonal velocity in m s^{-1} associated with the streamfunction ψ_f.

4. The unforced-undamped case

We will now apply the general results obtained in section 2 to the spectrally truncated system discussed in the previous section. To place our work in the perspective of known results, we consider in this section the case in which the system is neither forced nor damped. In the next section we consider the case in which both forcing and damping are present.

a. Analytical expressions

The constraints to be used in the maximization of the entropy when there is neither forcing nor damping are the expected values of the energy E and enstrophy Z:

$$\langle \mathcal{K}_1 \rangle = \langle E \rangle = E^0 \quad \text{and} \quad \langle \mathcal{K}_2 \rangle = \langle Z \rangle = Z^0, \qquad (54)$$

where E^0 and Z^0 are given values. The corresponding Lagrange multipliers will be denoted by $\lambda_1 = \alpha$ and $\lambda_2 = \beta$. All coefficients in the general expression of $\mathcal{K}_1$ are zero except for the coefficients $A_{1mn} = \frac{1}{2}\varepsilon_n$. For the coefficients of $\mathcal{K}_2$ we have $A_{2mn} = \frac{1}{2}\varepsilon_n^2$, $B_{2mn} = -\varepsilon_n f_{mn}$, and $C_{2mn} = \frac{1}{2} f_{mn}^2$. For the multivariate probability density function (22) that results from the maximization of entropy, we get

$$\mathcal{P}(\psi_{-N,-N}, \ldots, \psi_{N,N}) = \prod_{mn} \mathcal{N}(\mu_{mn}, \sigma_{mn}, \psi_{mn}), \qquad (55)$$

where the variance and mean follow from the general expressions [(17)]

$$\sigma_{mn}^2 = \frac{1}{\varepsilon_n(\alpha + \beta\varepsilon_n)} \quad \text{and} \quad \mu_{mn} = \frac{\beta f_{mn}}{\alpha + \beta\varepsilon_n}. \qquad (56)$$

Apart from dependence on the Lagrange multipliers α and β, the variance depends only on ε_n, whereas the mean values are determined by the Coriolis parameter, the orography, and ε_n. To find the values of α and β we consider the expectation values of the energy and enstrophy. Using $\langle \psi_{mn}^2 \rangle = \sigma_{mn}^2 + \mu_{mn}^2$ and $\langle \psi_{mn} \rangle = \mu_{mn}$, we find that

$$\langle E \rangle = \sum_{mn} \frac{1}{2}\varepsilon_n \langle \psi_{mn}^2 \rangle = \sum_{mn} \frac{1}{2}\varepsilon_n (\sigma_{mn}^2 + \mu_{mn}^2) \quad \text{and} \qquad (57a)$$

$$\begin{aligned} \langle Z \rangle &= \sum_{mn} \left[\frac{1}{2}\varepsilon_n^2 \langle \psi_{mn}^2 \rangle - \varepsilon_n f_{mn} \langle \psi_{mn} \rangle + \frac{1}{2} f_{mn}^2 \right] \\ &= \sum_{mn} \left[\frac{1}{2}\varepsilon_n^2 (\sigma_{mn}^2 + \mu_{mn}^2) - \varepsilon_n f_{mn} \mu_{mn} + \frac{1}{2} f_{mn}^2 \right]. \end{aligned} \qquad (57b)$$

When we substitute the expressions (56) for σ_{mn}^2 and μ_{mn} we get

$$\langle E \rangle = \sum_{mn} \left[\frac{1}{2(\alpha + \beta\varepsilon_n)} + \frac{\beta^2 \varepsilon_n f_{mn}^2}{2(\alpha + \beta\varepsilon_n)^2} \right], \qquad (58a)$$

$$\langle Z\rangle = \sum_{mn}\left[\frac{\varepsilon_n}{2(\alpha+\beta\varepsilon_n)} + \frac{\alpha^2 f_{mn}^2}{2(\alpha+\beta\varepsilon_n)^2}\right]. \quad (58b)$$

We have, without further approximation, if we assume that $\psi_{00} = 0$,

$$\langle E\rangle = \sum_{n=1}^{N} E_n \quad \text{and} \quad (59a)$$

$$\langle Z\rangle = \sum_{n=1}^{N} Z_n, \quad (59b)$$

in which the energy and enstrophy spectra E_n and Z_n are given by

$$E_n = \sum_{m=-n}^{n}\left[\frac{1}{2(\alpha+\beta\varepsilon_n)} + \frac{\beta^2\varepsilon_n f_{mn}^2}{2(\alpha+\beta\varepsilon_n)^2}\right] \quad \text{and} \quad (60a)$$

$$Z_n = \sum_{m=-n}^{n}\left[\frac{\varepsilon_n}{2(\alpha+\beta\varepsilon_n)} + \frac{\alpha^2 f_{mn}^2}{2(\alpha+\beta\varepsilon_n)^2}\right]. \quad (60b)$$

Because ε_n is independent of m, we can write

$$E_n = \frac{2n+1}{2(\alpha+\beta\varepsilon_n)} + \frac{\beta^2\varepsilon_n}{2(\alpha+\beta\varepsilon_n)^2}\sum_{m=-n}^{n} f_{mn}^2 \quad \text{and} \quad (61a)$$

$$Z_n = \frac{(2n+1)\varepsilon_n}{2(\alpha+\beta\varepsilon_n)} + \frac{\alpha^2}{2(\alpha+\beta\varepsilon_n)^2}\sum_{m=-n}^{n} f_{mn}^2. \quad (61b)$$

If the Coriolis parameter and the orography are assumed to be zero, we see from (58a), by taking $\beta = 0$, that there would be equipartition of energy among all the spectral coefficients if the energy were the only constraint in the maximization of entropy. The same is seen to be true, by taking $\alpha = 0$ in (58b), for the enstrophy if the enstrophy were the only constraint in the maximization of entropy. This is an expression of the equipartition theorem in equilibrium statistical mechanics. Under the same circumstances (i.e., when the Coriolis parameter and the orography are zero), E_n and Z_n behave as n^{-1} and n, respectively, for large n. In the context of two-dimensional turbulence these results are well known. For $f_{mn} = 0$ the results are in accord with Eq. (3.18) from the review by Kraichnan and Montgomery (1980), taking into account the difference in notation. The expressions (58a) and (58b) are identical to Eqs. (2.10a) and (2.10b) of Frederiksen and Sawford (1981), their h_{mn} corresponding to our f_{mn}, and are also in accord with Eqs. (3.8a) and (3.8b) of Carnevale and Frederiksen (1987), noting that ε_n reduces to e_n if $\Lambda = 0$.

TABLE 1. The forcing and damping parameters of the different numerical runs. A dash indicates that the tabled parameter is not relevant.

Run	Type	r	ν_{-1}	ν_r
1	Unforced–undamped	—	—	—
2	Damped	1	0	1.758×10^{-5}
3	Forced–damped	1	1.764×10^{-1}	1.758×10^{-5}

b. Numerical calculations

To check these results we did an integration with the numerical model without forcing or damping and with an initial state of which the field $\zeta - \Lambda\psi$ is given by

$$\zeta(\lambda,\phi) - \Lambda\psi(\lambda,\phi) = A_{25,25}Y_{25,25}(\lambda,\phi) + A_{26,26}Y_{26,26}(\lambda,\phi), \quad (62)$$

where $A_{25,25}$ and $A_{26,26}$ are both taken to be $1/\sqrt{2}$. The name and settings of this run are given in the first row of Table 1. We integrate the system for a total period of 2000 days, storing the output of the integration every 12 h. The relative vorticity field ζ at time $t = 0$ and $t =$ 2000 days are shown in Fig. 2. The meridionally aligned vortices, neatly arranged at $t = 0$, start to interact immediately and the field becomes turbulent very rapidly. After 100 days the system is already close to a statistically stationary state. By averaging over the last 1000 days of the 2000-day integration, which amounts to an average over 2000 fields, we obtained the energy and enstrophy spectra that are shown in Fig. 3. The numerical spectra of the energy and enstrophy are denoted by solid dots and open circles, respectively, and are calculated by averaging over

$$E_n = \sum_{m=-n}^{n}\frac{1}{2}\varepsilon_n\psi_{mn}^2 \quad \text{and} \quad (63a)$$

$$Z_n = \sum_{m=-n}^{n}\left(\frac{1}{2}\varepsilon_n^2\psi_{mn}^2 - \varepsilon_n f_{mn}\psi_{mn} + \frac{1}{2}f_{mn}^2\right), \quad (63b)$$

where the values of ψ_{mn} are obtained from the numerical integration.

The energy E^0 and enstrophy Z^0 of this integration are given in the first row of Table 2. These values are also averages over the last 1000 days of the integration, but because these quantities are conserved very accurately by the numerical model, they are virtually identical to their initial values. Using the procedure described in the appendix, we determined the maximum entropy spectrum by determining the Lagrange multipliers α and β from these values, yielding values that are given in the first row of Table 3. We then calculated the

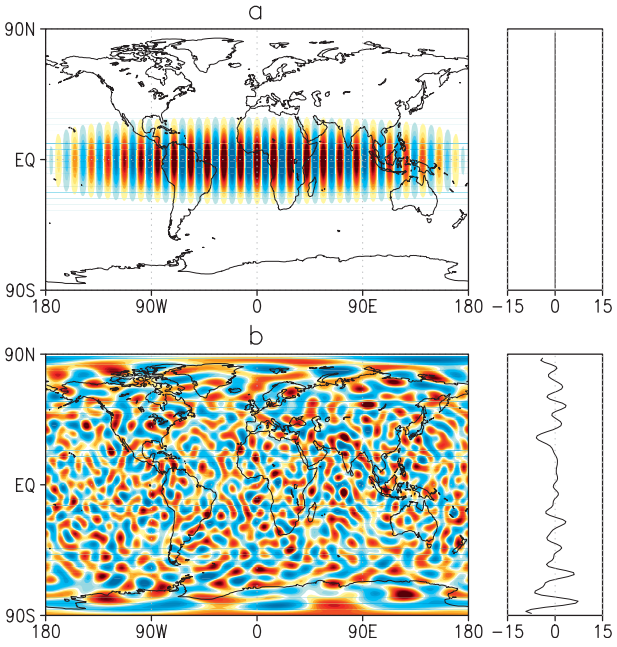

FIG. 2. The relative vorticity field at times (a) $t = 0$ and (b) $t =$ 2000 days in a numerical run without forcing or dissipation. The fields are displayed with a contour interval of 0.2; values in the range $(-0.1, 0.1)$ are colored white, values in the range $(0.1, 0.3)$ are colored light yellow, values in the range $(-0.3, -0.1)$ light blue, etc. The field in (a) lies in the range $(-4.2, 4.2)$ and the field in (b) lies in the range $(-3.7, 4.3)$. In all figures of this type, if we display the relative vorticity field with a contour interval of c, then values in the range $(-c/2, c/2)$ are colored white, values in the range $(c/2, 3c/2)$ are colored light yellow, values in the range $(-3c/2, -c/2)$ are light blue, etc. The profiles to the right of the relative vorticity fields show the zonally averaged zonal velocity (m s^{-1}).

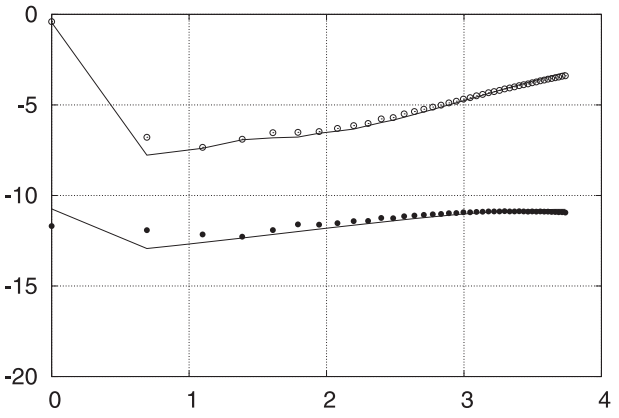

FIG. 3. The values of log E_n (energy) and log Z_n (enstrophy) as a function of log n, averaged over the last 1000 days of the 2000-day time integration of the unforced-undamped system. The numerical energy spectra are represented by solid dots and the numerical enstrophy spectra by open circles. The solid curves are the theoretical spectra, based on maximum entropy.

theoretical spectra for the energy and enstrophy; these are displayed by the solid lines in Fig. 3. We see that the theoretical spectra agree well with the numerical ones. The theoretical expected energy and enstrophy agree with the numerical values to within the accuracy with which these values are given, as can be checked by consulting the first row of Table 4.

In Fig. 4a we show the relative vorticity field averaged over the last 1000 days of the numerical integration. This average relative vorticity field may be compared to the theoretical expected relative vorticity field (referred to as the theoretical average) that can be calculated from

$$\langle \zeta \rangle = \sum_{mn} \langle \zeta_{mn} \rangle Y_{mn} = \sum_{mn} e_n \langle \psi_{mn} \rangle Y_{mn} = \sum_{mn} e_n \mu_{mn} Y_{mn}. \tag{64}$$

If we substitute the value of μ_{mn} as given by (56), using the values of α and β given in Table 3, we get the theoretical average relative vorticity field that is displayed in Fig. 4b. It should be remarked that the numerically calculated average relative vorticity field, displayed in Fig. 4a, has not completely converged and is therefore rather noisy. The theoretical average relative vorticity field, however, captures a few of the most important features, such as the regions of low and high relative vorticity over Greenland and Antarctica. The zonally averaged zonal velocity profiles, plotted to the right of the relative vorticity fields, show that the zonal flow is predominantly easterly in the numerical average. This is also in accordance with the theoretical average, which is dominated by an easterly solid-body rotation.

5. The forced-damped case

The results of the previous section have confirmed that the statistics of a system that is neither damped nor forced and has been left to itself for a sufficiently long time are determined by its energy and enstrophy. If the system is damped but not forced and thus decays freely in time, one might conjecture that the decay rates of energy and enstrophy are also important in determining the statistics of the system. In the same way, if both forcing and damping act on the system and the system has reached a statistically stationary state, then the

TABLE 2. The energy E^0, enstrophy Z^0, decay rate of energy $-dE^0/dt$, and decay rate of enstrophy $-dZ^0/dt$ of the different runs, the parameters of which are summarized in Table 1.

Run	E^0	Z^0	$-dE^0/dt$	$-dZ^0/dt$
1	6.450×10^{-4}	$1.215 \times 10^{+0}$	—	—
2	1.739×10^{-4}	7.065×10^{-1}	6.426×10^{-7}	4.173×10^{-4}
3	1.105×10^{-3}	$1.327 \times 10^{+0}$	2.234×10^{-10}	6.006×10^{-8}

TABLE 3. The Lagrange multipliers for the different entropy maximizations.

Run	α	β	γ	δ
1	$+9.779 \times 10^{5}$	$+5.444 \times 10^{2}$	—	—
2	$+4.166 \times 10^{6}$	$+3.807 \times 10^{3}$	—	—
2	—	—	$+9.608 \times 10^{7}$	$+2.048 \times 10^{6}$
2	$+5.040 \times 10^{5}$	$+1.770 \times 10^{2}$	-3.965×10^{8}	$+2.578 \times 10^{6}$
3	$+4.075 \times 10^{5}$	$+6.638 \times 10^{2}$	—	—
3	—	—	$+3.757 \times 10^{8}$	$+7.468 \times 10^{5}$
3	$+3.274 \times 10^{6}$	-2.943×10^{4}	-1.765×10^{9}	$+1.668 \times 10^{7}$

condition that the decay rates of energy and enstrophy are zero might be important for the statistics of the system. The latter idea was put forward and explored by Burgers (1939) and will be investigated further in the present section. We first consider the case in which the decay rates of energy and enstrophy are used as the only constraints in the maximization of entropy. We will see that the procedure is very similar to the procedure discussed above. We will then describe the procedure in the case where the decay rates of energy and enstrophy are combined with the energy and enstrophy themselves.

a. Analytical expressions

First, we will consider as constraints, with respective Lagrange multipliers $\lambda_3 = \gamma$ and $\lambda_4 = \delta$,

$$\langle \mathcal{K}_3 \rangle = \langle \mathcal{D} - \mathcal{F} \rangle = \mathcal{D}^0, \quad \langle \mathcal{K}_4 \rangle = \langle \mathcal{H} - \mathcal{G} \rangle = \mathcal{H}^0. \tag{65}$$

As already noted, these constraints are also of the general form (14). For the corresponding coefficients we have $A_{3mn} = d_n$, $B_{3mn} = F_{mn}$, $C_{3mn} = 0$, $A_{4mn} = d_n\varepsilon_n$, $B_{4mn} = \varepsilon_n F_{mn} - d_n f_{mn}$, and $C_{4mn} = -f_{mn}F_{mn}$. This gives the probability density function

$$\mathcal{P}(\psi_{-N,-N}, \ \ldots, \psi_{N,N}) = \prod_{mn} \mathcal{N}(\mu_{mn}, \sigma_{mn}, \psi_{mn}), \tag{66}$$

where, using (17), the variance and mean are

$$\sigma_{mn}^2 = \frac{1}{2d_n(\gamma + \delta\varepsilon_n)}, \quad \mu_{mn} = \frac{\delta f_{mn}}{2(\gamma + \delta\varepsilon_n)} - \frac{F_{mn}}{2d_n}. \tag{67}$$

The difference from the unforced-undamped case is in the dependence of σ_{mn}^2 on d_n and the addition of an extra term (due to the forcing) in the expression of μ_{mn}. As before, to find the values of γ and δ we consider the expectation values of the constraints:

$$\begin{aligned}\langle \mathcal{D} - \mathcal{F} \rangle &= \sum_{mn} (d_n \langle \psi_{mn}^2 \rangle + F_{mn} \langle \psi_{mn} \rangle) \\ &= \sum_{mn} [d_n(\sigma_{mn}^2 + \mu_{mn}^2) + F_{mn}\mu_{mn}], \quad \text{and} \end{aligned} \tag{68a}$$

$$\begin{aligned}\langle \mathcal{H} - \mathcal{G} \rangle &= \sum_{mn} [d_n\varepsilon_n \langle \psi_{mn}^2 \rangle + (\varepsilon_n F_{mn} - d_n f_{mn}) \langle \psi_{mn} \rangle \\ &\quad - f_{mn}F_{mn}] \\ &= \sum_{mn} [d_n\varepsilon_n(\sigma_{mn}^2 + \mu_{mn}^2) + (\varepsilon_n F_{mn} - d_n f_{mn})\mu_{mn} \\ &\quad - f_{mn}F_{mn}]. \end{aligned} \tag{68b}$$

If we substitute the expressions for σ_{mn}^2 and μ_{mn}, given by (67), we get

$$\langle \mathcal{D} - \mathcal{F} \rangle = \sum_{mn} \left[\frac{1}{2(\gamma + \delta\varepsilon_n)} + \frac{\delta^2 d_n f_{mn}^2}{4(\gamma + \delta\varepsilon_n)^2} - \frac{F_{mn}^2}{4d_n} \right] \quad \text{and} \tag{69a}$$

$$\begin{aligned}\langle \mathcal{H} - \mathcal{G} \rangle = \sum_{mn} \Bigg[&\frac{\varepsilon_n}{2(\gamma + \delta\varepsilon_n)} - \frac{\delta(\delta\varepsilon_n + 2\gamma) d_n f_{mn}^2}{4(\gamma + \delta\varepsilon_n)^2} \\ &- \frac{\varepsilon_n F_{mn}^2}{4d_n} - \frac{f_{mn}F_{mn}}{2} \Bigg]. \end{aligned} \tag{69b}$$

In the freely decaying case these expressions should be set equal to the given values of $\mathcal{D}^0$ and $\mathcal{H}^0$. If forcing is present and if we consider a statistically stationary state, we set these expectation values to zero.

As in the unforced-undamped case, we have (57a) and (57b) for the energy and enstrophy. Substituting the expressions for σ_{mn}^2 and μ_{mn}, given by (67), this leads to

TABLE 4. The expectation values of the energy E, enstrophy Z, decay rate of energy $-dE/dt$, and decay rate of enstrophy $-dZ/dt$.

Run	$\langle E \rangle$	$\langle Z \rangle$	$-\langle dE/dt \rangle$	$-\langle dZ/dt \rangle$
1	6.450×10^{-4}	$1.215 \times 10^{+0}$	—	—
2	1.739×10^{-4}	7.065×10^{-1}	4.054×10^{-6}	2.874×10^{-3}
2	5.623×10^{-3}	8.313×10^{-1}	6.426×10^{-7}	4.173×10^{-4}
2	1.739×10^{-4}	7.065×10^{-1}	6.426×10^{-7}	4.173×10^{-4}
3	1.105×10^{-3}	$1.327 \times 10^{+0}$	2.463×10^{-5}	2.680×10^{-2}
3	2.563×10^{-4}	9.118×10^{-1}	2.613×10^{-22}	-1.983×10^{-13}
3	1.105×10^{-3}	$1.327 \times 10^{+0}$	6.511×10^{-11}	-3.243×10^{-17}

$$\langle E\rangle = \sum_{mn}\left[\frac{\varepsilon_n}{4d_n(\gamma+\delta\varepsilon_n)} + \varepsilon_n\frac{\{\delta f_{mn} - [(\gamma+\delta\varepsilon_n)F_{mn}]/d_n\}^2}{8(\gamma+\delta\varepsilon_n)^2}\right] \quad \text{and} \tag{70a}$$

$$\langle Z\rangle = \sum_{mn}\left[\frac{\varepsilon_n^2}{4d_n(\gamma+\delta\varepsilon_n)} + \frac{\{(\delta\varepsilon_n+2\gamma)f_{mn} + [(\gamma+\delta\varepsilon_n)\varepsilon_n F_{mn}]/d_n\}^2}{8(\gamma+\delta\varepsilon_n)^2}\right]. \tag{70b}$$

Assuming as before that $\psi_{00} = 0$, these expressions can be written as

$$\langle E\rangle = \sum_{n=1}^{N} E_n \quad \text{and} \tag{71a}$$

$$\langle Z\rangle = \sum_{n=1}^{N} Z_n, \tag{71b}$$

where, because both ε_n and d_n are independent of m, we have

$$E_n = \frac{(2n+1)\varepsilon_n}{4d_n(\gamma+\delta\varepsilon_n)} + \frac{\varepsilon_n}{8(\gamma+\delta\varepsilon_n)^2}\sum_{m=-n}^{n}\{\delta f_{mn} - [(\gamma+\delta\varepsilon_n)F_{mn}]/d_n\}^2 \quad \text{and} \tag{72a}$$

$$Z_n = \frac{(2n+1)\varepsilon_n^2}{4d_n(\gamma+\delta\varepsilon_n)} + \frac{1}{8(\gamma+\delta\varepsilon_n)^2}\sum_{m=-n}^{n}\{(\delta\varepsilon_n+2\gamma)f_{mn} + [(\gamma+\delta\varepsilon_n)\varepsilon_n F_{mn}]/d_n\}^2. \tag{72b}$$

We see from (69a) that with zero Coriolis parameter, orography, and forcing, and considering only the dissipation of energy (so that the Lagrange multiplier δ is zero), all spectral components contribute equally to the dissipation of energy. This is Burgers' equipartition of dissipation, referred to in the introduction. Similarly, if only the dissipation of enstrophy is considered (so that the Lagrange multiplier γ is zero), all spectral components contribute equally to the dissipation of enstrophy, as can be seen from (69b). Furthermore, if there is only Newtonian viscosity ($r = 1$), so that $d_n = \nu_1 e_n^2 \sim n^4$ and the Coriolis parameter and the orography are zero, then E_n and Z_n behave as n^{-3} and n^{-1}, respectively, for large values of n. If there is only hyperviscosity ($r = 2$), then E_n and Z_n behave as n^{-5} and n^{-3}, respectively. More generally, we see from the definition of d_n that the behavior of E_n and Z_n for large n is determined by the highest-order damping present. We note that the energy spectrum $E_n \sim n^{-3}$, in the case of Newtonian viscosity ($r = 1$), is identical to the spectrum obtained in the enstrophy inertial range for two-dimensional turbulence [see Eq. (4.12) of Kraichnan and Montgomery 1980]. The energy spectrum $E_n \sim n^{-5}$ in the case of hyperviscosity ($r = 2$) does agree with the spectrum that is obtained by McWilliams (1984) in his simulations of decaying two-dimensional turbulence with hyperviscosity (see his Fig. 2). All this indicates that the results obtained are not unrealistic.

It is also possible to use both the energy and enstrophy as well as their decay rates (which are, as we

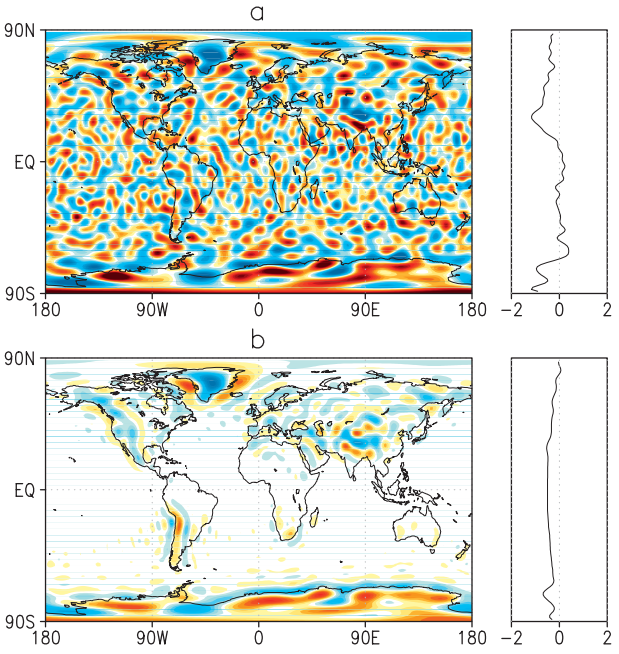

FIG. 4. (a) The relative vorticity averaged over the last 1000 days of the integration of the unforced-undamped system. (b) The expected relative vorticity field based on maximum entropy. The fields are displayed with a contour interval of 0.01, where the field in (a) lies in the range (−0.19, 0.18) and the field in (b) lies in the range (−0.11, 0.08). The profiles to the right show that the zonally averaged zonal velocity of the numerical average is predominantly easterly, in accordance with the theoretical average, although the numerical average is rather noisy because of incomplete convergence. The correlation coefficient between the relative vorticity fields in (a) and (b) is 0.41. This coefficient (and the coefficients mentioned in the captions of Figs. 7 and 10) is calculated on the basis of the 256 × 128 values that are plotted, weighted by the cosine of the latitude.

emphasize, zero in the statistically stationary state) in the maximization of entropy. We then require

$$\langle \mathcal{K}_1 \rangle = \langle E \rangle = E^0, \qquad \langle \mathcal{K}_2 \rangle = \langle Z \rangle = Z^0, \quad (73)$$

$$\langle \mathcal{K}_3 \rangle = \langle \mathcal{D} - \mathcal{F} \rangle = \mathcal{D}^0, \quad \text{and} \quad \langle \mathcal{K}_4 \rangle = \langle \mathcal{H} - \mathcal{G} \rangle = \mathcal{H}^0. \quad (74)$$

Denoting the corresponding Lagrange multipliers by α, β, γ, and δ and using the general expressions given in section 2, we obtain a product of normal distribution functions with the following expressions of σ_{mn} and μ_{mn}:

$$\sigma_{mn}^2 = \frac{1}{\varepsilon_n(\alpha + \beta\varepsilon_n) + 2d_n(\gamma + \delta\varepsilon_n)}, \quad \text{and} \quad (75)$$

$$\mu_{mn} = \frac{(\beta\varepsilon_n + \delta d_n) f_{mn} - (\gamma + \delta\varepsilon_n) F_{mn}}{\varepsilon_n(\alpha + \beta\varepsilon_n) + 2d_n(\gamma + \delta\varepsilon_n)}. \quad (76)$$

The expressions of $\langle E \rangle$, $\langle Z \rangle$, $\langle \mathcal{D} - \mathcal{F} \rangle$, and $\langle \mathcal{H} - \mathcal{G} \rangle$ become too involved to write out explicitly but can be handled numerically without any problems. Calculating the Lagrange multipliers from given expectation values is discussed in the appendix.

b. Numerical calculations—Damped

In the second experiment with the numerical model, of which the parameters are given in the second row of Table 1, we use the last 100 fields of the previous integration as initial conditions for an ensemble of 100 integrations over a period of 20 days. Here, however, we added a Newtonian viscosity term ($r = 1$) with $\tau_r = 5$ days (giving $\nu_r = 1.758 \times 10^{-5}$). We thus consider a case in which a turbulent system decays freely under the action of Newtonian viscosity. The relative vorticity at time $t =$ 10 and $t = 20$ days for the last member of the ensemble are shown in Fig. 5. When we compare the two panels in this figure with Fig. 2b, we see how in the course of time the dominant spatial scales become larger, a well-known fact in freely decaying two-dimensional turbulence (McWilliams 1984). This is also demonstrated by the numerical spectra of energy (solid dots) and enstrophy (open circles) at time $t = 20$ days that are shown in Fig. 6. These spectra are obtained by using (63a) and (63b) and averaging over the 100 members of the ensemble.

The solid lines in Fig. 6 represent three different theoretical spectra. The theoretical spectra in Fig. 6a are obtained by maximizing the entropy, keeping the energy and enstrophy fixed at the values E^0 and Z^0 at time $t = 20$ days, obtained from the numerical experiment by averaging over the ensemble and given in the second row of Table 2. We give these spectra as a reference to show that the spectra after 20 days are quite far from the

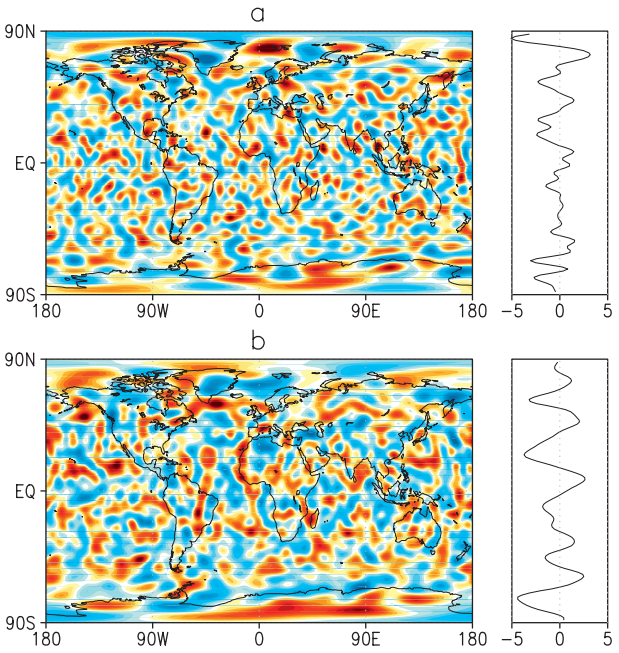

FIG. 5. The relative vorticity field at times (a) $t = 10$ days and (b) $t = 20$ days of member 100 of an ensemble of flows decaying freely as the result of Newtonian viscosity. The field in (a) lies in the range $(-1.6, 1.4)$ and is plotted with a contour interval of 0.1; the field in (b) lies in the range $(-0.7, 0.7)$ and is plotted with a contour interval of 0.05. By comparing the fields in (a) and (b) with the field in Fig. 2b, we see how the dominant spatial scales become larger in the process of decay. This is also clear from the zonally averaged zonal velocity profiles (m s^{-1}), displayed to the right of the relative vorticity fields.

inviscid equilibrium spectra encountered in the previous section. The theoretical spectra in Fig. 6b are obtained by maximizing the entropy, keeping the energy and enstrophy dissipation rates fixed at the values $-dE^0/dt = \mathcal{D}^0$ and $-dZ^0/dt = \mathcal{H}^0$, also obtained by averaging over the ensemble and given in the second row of Table 2. The correspondence is now better, in particular at the higher wavenumbers where the slopes of the numerical spectra are well represented. At the lower wavenumbers the spectra still deviate rather much from the numerically obtained results. In Fig. 6c we show the spectra that result when entropy is maximized, keeping the energy and enstrophy and also their decay rates fixed at the values obtained from the numerical experiment. Now the spectra at lower wavenumbers are also well described.

The relative vorticity field at time $t = 20$ days, averaged over the 100 members of the ensemble, is shown in Fig. 7a. Even for as few as 100 members, the average has converged better than the average in the unforced-undamped case, although there is still considerable noise left. In Fig. 7b we show the theoretical average

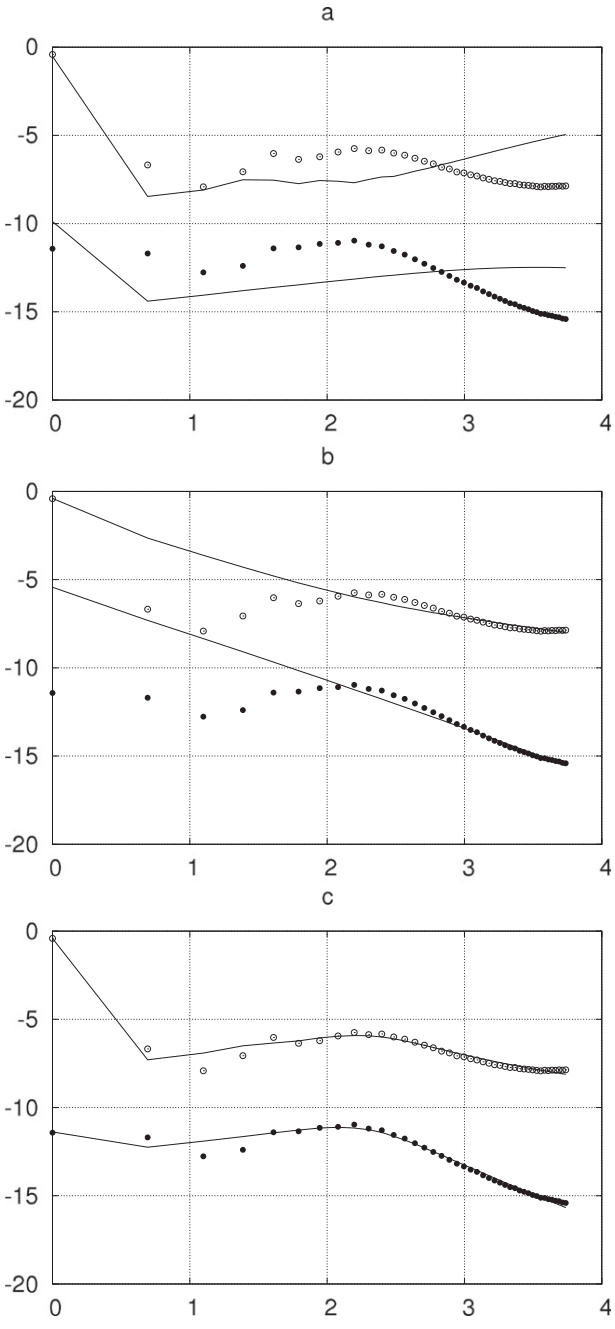

FIG. 6. The values of log E_n (energy) and log Z_n (enstrophy) as functions of log n, averaged over an ensemble of 100 fields at 20 days after the damping has set in. The solid dots represent the spectra of energy, the open circles represent the spectra of enstrophy, and the solid curves are the theoretical spectra, based on maximum entropy. The constraints in the maximization of entropy are (a) energy and enstrophy, (b) the decay rates of energy and enstrophy, and (c) energy and enstrophy as well as their decay rates. The slope of the numerically obtained energy spectra at the high end of the spectrum is around −3.1.

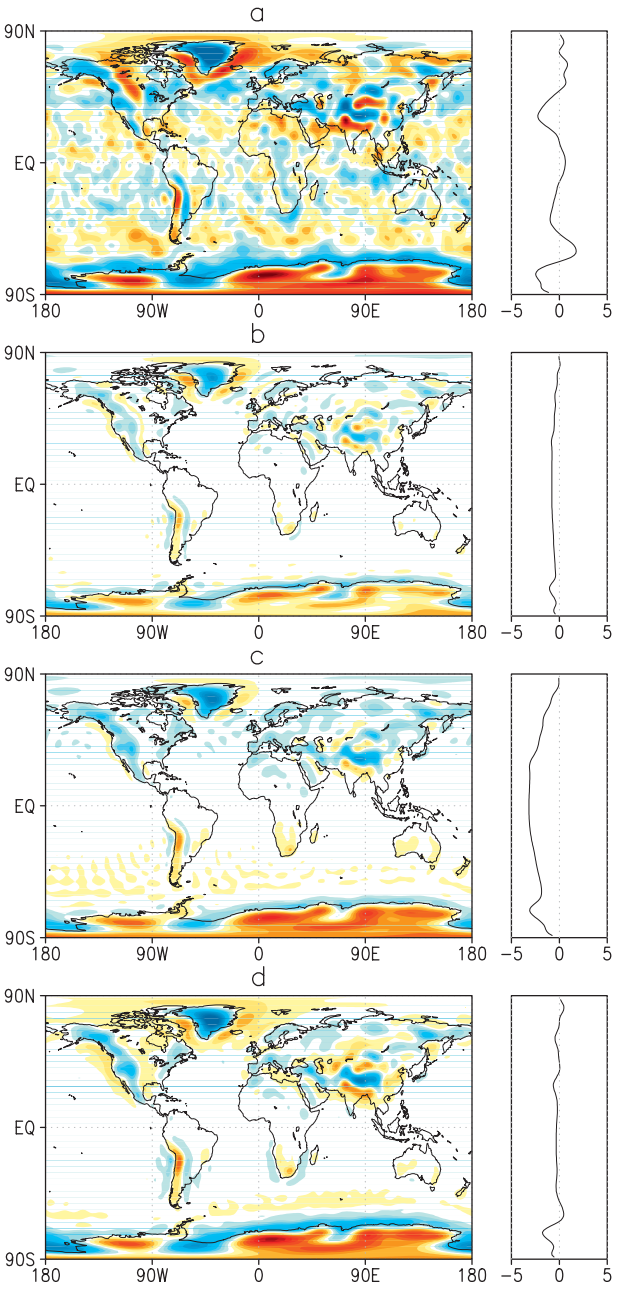

FIG. 7. Relative vorticity fields displayed with a contour interval of 0.02. (a) The relative vorticity averaged over the 100 members of the ensemble, 20 days after the damping has set in. (b)–(d) The theoretical expected relative vorticity, based on maximization of entropy; the constraints are (b) energy and enstrophy, (c) the decay rates of energy and enstrophy, and (d) both energy and enstrophy and their decay rates. The fields in the consecutive panels vary between (−0.43, 0.22), (−0.15, 0.11), (−0.21, 0.16), and (−0.28, 0.20), respectively. The profiles to the right display the zonally averaged zonal velocity (m s^{-1}). The correlation coefficients between the relative vorticity fields in (a) and (b), (a) and (c), and (a) and (d) are 0.70, 0.66, and 0.71, respectively.

based on maximizing the entropy with the given energy and enstrophy as constraints. In Fig. 7c the theoretical average is shown for the case in which the decay rates are used as constraints, whereas in Fig. 7d the theoretical average is shown for the case in which energy and enstrophy as well as their decay rates are used as constraints. We see that along with the spectra, the correspondence with the numerical results improves between Figs. 7b and 7d.

The different Lagrange multipliers and the corresponding theoretical expectation values of energy, enstrophy, and their decay rates are given in the second, third, and fourth rows of the Tables 3 and 4. For completeness we also give in Table 4 the expected decay rates of energy and enstrophy when entropy is maximized with energy and enstrophy as constraints (second row) and the energy and enstrophy when entropy is maximized with only the decay rates as constraints (third row). The fourth row shows that all four quantities are reproduced accurately if all these quantities are kept fixed in the maximization of entropy.

c. *Numerical calculations—Forced-damped*

In the third experiment, in which the system is spun up from an initial state of rest, both forcing and damping act on the system. To the viscosity term of the damped case we add the term $\nu_{-1}(\psi - \psi_f)$, where $\nu_{-1} = 1.764 \times 10^{-1}$, corresponding to $\tau_{-1} = 90$ days in (52). The parameters are given in the third row of Table 1. As in the first experiment, the run is 2000 dimensional days long. The graphs of energy, enstrophy, and their forcing and damping rates (not shown) reveal that the system reaches a dynamical equilibrium after about 500 days. The energy E^0, enstrophy Z^0, energy decay rate $-dE^0/dt = \mathcal{D}^0 - \mathcal{F}^0$, and enstrophy decay rate $-dZ^0/dt = \mathcal{H}^0 - \mathcal{G}^0$, based on averaging over the last 500 days (1000 fields) of the integration, are given in the third row of Table 2. To give an idea of the amount of variability in the statistically stationary state, we show in Fig. 8 snapshots of the flow at two times, 10 days apart, at the end of the integration period (the second snapshot is at time $t = 2000$ days).

The spectra, averaged over the last 500 days of the integration, are shown in Fig. 9. As before, the solid dots and open circles denote the numerical energy and enstrophy spectra, respectively, whereas the solid lines denote the theoretical spectra. As in the freely damped case, the three panels of the figure contain identical numerical results, whereas the different theoretical curves are spectra based on different constraints in the maximization of entropy. The theoretical curves in Fig. 9a are based on maximum entropy, keeping the energy and enstrophy fixed at the values obtained from the numerical experiment. We see that there is a large difference between the numerical and theoretical spectra, signifying that the forced-damped system is far from inviscid equilibrium. In Fig. 9b the theoretical spectra are shown for the case in which the entropy is maximized with the decay rates of energy and enstrophy fixed at the value zero. From Table 2 we see that the numerically obtained average decay rates are not exactly zero, but taking the values from the table instead of the value zero does not make a noticeable difference in the results. This particular case is quite interesting because here we do not need any information from the numerical experiment—the decay rates can be taken to be zero—to obtain a theoretical spectrum. In other words, the principle of maximum entropy is here purely predictive in the sense that the only information needed from the run is the fact that the system has reached a statistically stationary state. However, although the correspondence is better than in the first case, there remain notable differences, especially at the higher wavenumbers. When zero decay rates of energy and enstrophy are used in combination with the (numerically obtained) values of the energy and enstrophy, the correspondence improves, but there still remain differences between the theoretical and numerical spectra.

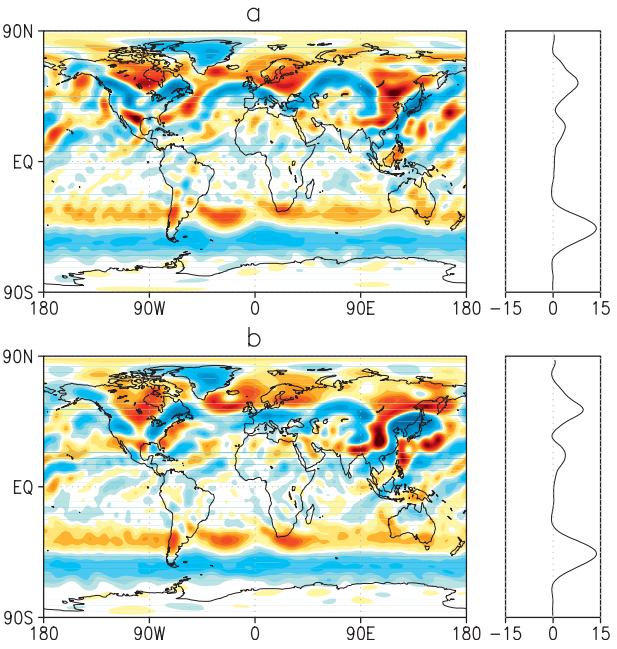

FIG. 8. The relative vorticity field at times (a) $t = 1990$ days and (b) $t = 2000$ days in a numerical run with forcing and dissipation. The values are in the range $(-0.50, 0.55)$ and $(-0.57, 0.61)$, respectively, and are displayed with a contour interval of 0.04. The profiles to the right of the relative vorticity fields are the zonally averaged zonal velocity (m s^{-1}).

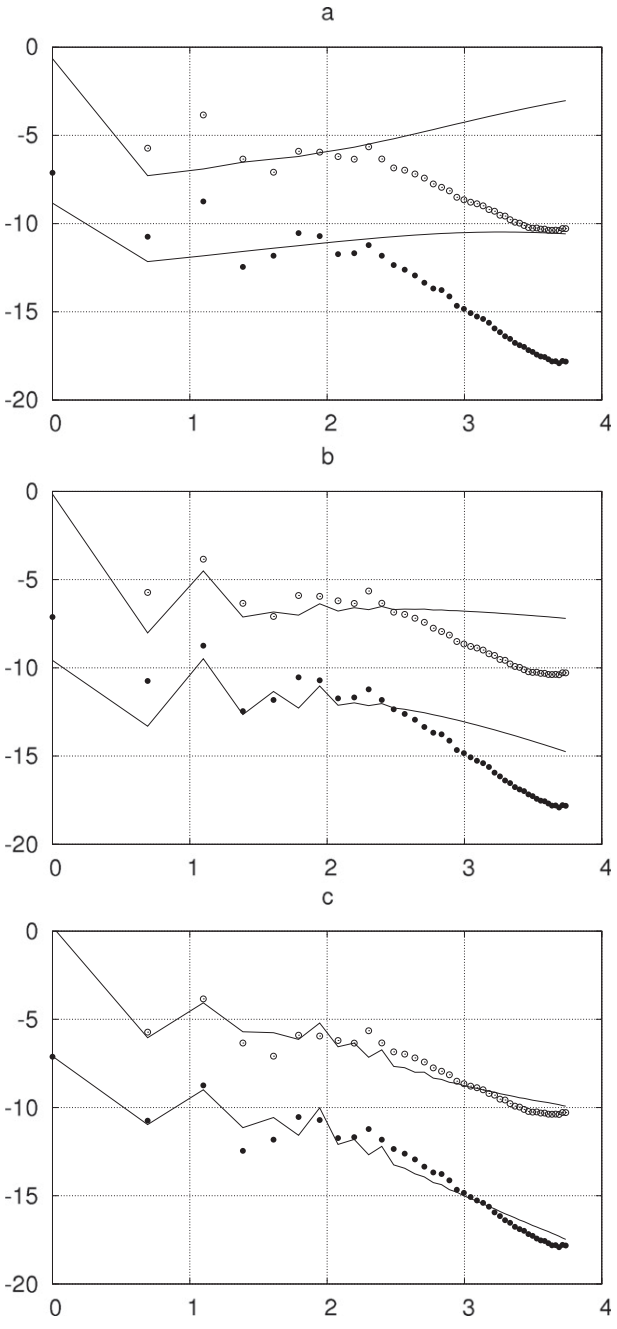

FIG. 9. The values of log E_n (energy) and log Z_n (enstrophy) as a function of log n, averaged over the last 500 days of the forced-damped run. The solid dots represent the spectra of energy, the open circles represent the spectra of enstrophy, and the solid curves are the theoretical spectra, based on maximum entropy. The constraints in the maximization of entropy are (a) energy and enstrophy, (b) the decay rates of energy and enstrophy (taken to be zero), and (c) both energy and enstrophy and their decay rates. The slope of the numerically obtained energy spectra at the high end of the spectrum is around -4.5.

This concerns, in particular, the slopes at high wavenumbers; see Fig. 9c.

In Fig. 10a we show the relative vorticity field averaged over the last 500 days of the integration. This field has converged perfectly and can be compared without qualifications to the expected relative vorticity fields obtained from the theory. In Fig. 10b we show the theoretical average for the case in which the entropy is maximized with the energy and enstrophy obtained from the experiment as constraints. In Fig. 10c the theoretical average is shown for the case in which the entropy is maximized using the (zero) decay rates of the energy and enstrophy as constraints. In Fig. 10d the energy and enstrophy as well as their (zero) decay rates are used as constraints in the maximization of entropy. Quite remarkable is that Fig. 10c shows that maximization of entropy, constrained by the (zero) decay rates of energy and enstrophy, predicts an average flow that contains a zonal flow component of the same basic structure as the zonal flow component in the numerical average. This can be seen quite clearly from the profiles shown to the right of the relative vorticity plots and is markedly different from the case displayed in Fig. 10b, in which the energy and enstrophy from the numerical run are used as constraints. Indeed, considering the profiles of zonally averaged zonal velocity, we see in Fig. 10b a rather weak zonal flow dominated by an easterly solid body rotation, whereas in Fig. 10c we clearly see the two jet streams that have developed as a result of the forcing. Maximizing the entropy with both energy and enstrophy as well as their (zero) decay rates improves the resemblance still further although discrepancies, such a lack of wavelike variability, still remain.

The different Lagrange multipliers and theoretical expected values for the energy, enstrophy, etc. are given in the last three rows of Tables 3 and 4. Also here we give in Table 4 the expected decay rates of energy and enstrophy when entropy is maximized with energy and enstrophy as constraints (fifth row) and the energy and enstrophy when entropy is maximized with only the (zero) decay rates as constraints (sixth row). The sixth row shows that if the entropy is maximized, constrained by the (zero) decay rates of energy and enstrophy, the resulting values of the energy and enstrophy are lower than the numerical values.

6. Conclusions and outlook

In this paper we have applied the principle of maximum entropy to the statistical mechanics of the equivalent barotropic vorticity equation on a sphere. The equivalent barotropic vorticity equation is a system that is frequently used as a first-order model of the general

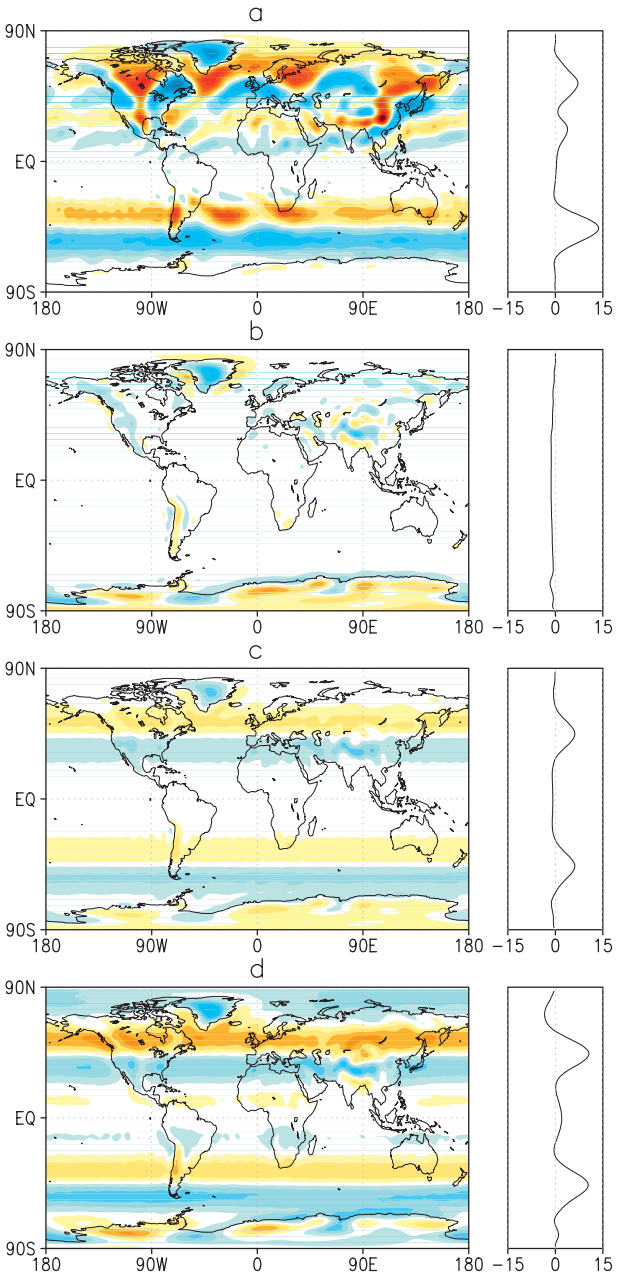

FIG. 10. Relative vorticity fields displayed with a contour interval of 0.04. (a) The relative vorticity averaged over the last 500 days of the 2000 days integration of the forced-damped system. (b)–(d) The theoretical expected relative vorticity, based on maximization of entropy; the constraints are (b) energy and enstrophy, (c) the (zero) decay rates of energy and enstrophy, and (d) both energy and enstrophy and their decay rates. The fields in the consecutive panels vary between (−0.41, 0.46), (−0.21, 0.15), (−0.13, 0.09), and (−0.21, 0.17). The correlation coefficients between the relative vorticity fields in (a) and (b), (a) and (c), and (a) and (d) are 0.20, 0.46, and 0.44, respectively.

circulation of the atmosphere. With suitable forcing and damping parameters, it displays the typical two-dimensional turbulent behavior that can be observed in the atmosphere, as demonstrated by Ambaum (1997). The turbulent nature of the atmosphere's general circulation leads quite naturally to a study of its properties with the techniques of statistical mechanics; see Salmon (1998). Until now, however, it was mostly equilibrium statistical mechanics that was applied, despite the presence of forcing and damping in the real atmosphere. In a more general fluid dynamical context, an important exception is the work of Burgers (1939), who went beyond equilibrium statistical mechanics in studying turbulent flows in which forcing and damping are prominently present. His idea was to apply the condition of an average compensation between input and output of the relevant conserved quantity (energy in his case) instead of a fixed value of the conserved quantity itself.

In the present paper we have taken up Burgers' thread again but have based it on the principle of maximum entropy, as put forward by Jaynes (1957a,b). In section 2 we summarized the technique of maximum entropy and applied it to general finite-dimensional systems with constraints that are quadratic in the variables. We derived general formulas that are then applied to the system that we introduce in section 3: the equivalent barotropic vorticity equation on a sphere. The results presented in section 4 have confirmed that if the unforced-undamped version of that system is left to itself for a time sufficiently long to reach a statistically stationary state, the statistics of that system are well captured by a probability density function based on maximum entropy with the system's expected energy and enstrophy as constraints. This was demonstrated by comparing the numerical energy and enstrophy spectra, obtained by averaging over 1000 days in the second half of a 2000-day-long numerical integration, with the corresponding maximum entropy spectra, both shown in Fig. 3. We also studied the numerical average of the relative vorticity field. Although averaging over 1000 days was not enough to achieve complete convergence, the most important features were captured reasonably well by the theoretical expected relative vorticity field, as can be verified by comparing Figs. 4a and 4b. These results are in accordance with the literature (see Frederiksen and Sawford 1981; Carnevale and Frederiksen 1987).

In section 5 we used the general formulas of section 2 to obtain the probability density function of a system if its entropy is maximized, constrained by the decay rates of energy and enstrophy or by these decay rates in combination with the energy and enstrophy themselves. We first studied an ensemble of 100 time integrations, starting from the last 100 stored fields of the inviscid

integration, unforced but with Newtonian viscosity as the damping mechanism. We studied the results after the damping had been effective for 20 days. The numerical spectra were obtained by averaging over the 100 members of the ensemble and are shown in Fig. 6. In Fig. 6a the solid lines denote the spectra based on maximum entropy, keeping the energy and enstrophy fixed. In Fig. 6b the solid lines denote maximum entropy spectra, based on fixed decay rates of energy and enstrophy. In Fig. 6c the solid curves are maximum entropy spectra, based on fixed decay rates of energy and enstrophy in combination with fixed values of energy and enstrophy. The latter theoretical spectra give a good description of the numerical spectra at both small and high values of the wavenumbers. In Fig. 7 we show that the numerical average relative vorticity field is represented increasingly better, along with the spectra. We thus conclude that both the energy and enstrophy and the decay rates of energy and enstrophy contain important information on the statistics of a freely decaying turbulent system and that this information can be exploited successfully by using the principle of maximum entropy.

It should be noted, however, that if the damping is allowed to be active for a longer time the results become less impressive. The numerical spectra, for instance, become steeper than the theoretical ones and also the numerical average fields are less well described by the expected fields based on maximum entropy. Examples were not given but the fact is illustrated well enough by the results of a forced-damped version of the model. Here, damping (and forcing) has been allowed to act for such a long time that the system has reached a state of statistical equilibrium, a state characterized by averages that do not change in time. The spectra and average relative vorticity fields, both numerical and theoretical, are shown in Figs. 9 and 10. In analogy to the previous case, we calculated maximum entropy spectra based on energy and enstrophy (taken from the simulation), (zero) decay rates of energy and enstrophy, and a combination of the two. Both theoretical spectra and average relative vorticity fields improve, going from energy/enstrophy as constraints to a combination of these with their (zero) decay rates, but there remain discrepancies, in particular concerning the slopes of the spectra and the amount of wave structure in the average flow.

The principle of maximum entropy, as we have applied it, has shown its most predictive side in the forced-damped case in which the (zero) decay rates of energy and enstrophy are used as constraints. Without any information from the numerical run, except for the fact that it has reached a statistically stationary state, it predicts a spectrum and expected relative vorticity field that match the numerical results better than the spectrum and expected relative vorticity field that are based on energy and enstrophy as constraints, with values taken from the numerical run. As we have seen, the results are improved if the (zero) decay rates of energy and enstrophy are combined with the energy and enstrophy from the numerical run. However, by using values from the numerical run, part of the theory's predictive power is lost and we might wonder whether it is possible to achieve improvements without reliance on the numerical run.

As a possible way forward, we might contemplate maximizing the entropy $\mathcal{S}_I$, constrained by fixed values of $\langle E\rangle$, $\langle Z\rangle$, $\langle dE/dt\rangle$, and $\langle dZ/dt\rangle$, but leaving the actual values of $\langle E\rangle$ and $\langle Z\rangle$ undetermined. The maximum entropy $\mathcal{S}_M$, as given by (29), would then become a function of $\langle E\rangle$ and $\langle Z\rangle$:

$$\mathcal{S}_M = \mathcal{S}_M\left(\langle E\rangle, \langle Z\rangle, \left\langle\frac{dE}{dt}\right\rangle, \left\langle\frac{dZ}{dt}\right\rangle\right), \tag{77}$$

because it is understood that the last two arguments of $\mathcal{S}_M$ are fixed at the value zero. Phrased in this way, the principle of maximum entropy states that the most appropriate values of $\langle E\rangle$ and $\langle Z\rangle$ are those values that maximize $\mathcal{S}_M$. A maximum exists, indeed, but will be attained by the values of $\langle E\rangle$ and $\langle Z\rangle$ that result from maximizing the entropy $\mathcal{S}_I$ without these quantities as constraints. The reason is that extra constraints can never increase the maximum value of a function, including the entropy.

The procedure above would thus yield the values of $\langle E\rangle$ and $\langle Z\rangle$ that are already given in the sixth row of Table 4. It would confirm that values of $\langle E\rangle$ and $\langle Z\rangle$, taken from the numerical run, do indeed provide additional information. However, additional information may also be extracted from the fact that the system is in a statistically stationary state. Indeed, for a statistically stationary state $\langle E\rangle$ and $\langle Z\rangle$ are, by definition, constant in time. This would suggest that if we permit ourselves to require that $\langle dE/dt\rangle$ and $\langle dZ/dt\rangle$ are zero, we may as well require that $\langle d^nE/dt^n\rangle$ and $\langle d^nZ/dt^n\rangle$ are zero for $n = 2, 3, \ldots$. These extra constraints are nontrivial. For $n = 2$ we have

$$\frac{d^2E}{dt^2} = \frac{d\mathcal{F}}{dt} - \frac{d\mathcal{D}}{dt} \quad \text{and} \tag{78a}$$

$$\frac{d^2Z}{dt^2} = \frac{d\mathcal{G}}{dt} - \frac{d\mathcal{H}}{dt}, \tag{78b}$$

as follows straightforwardly from the budget equations [(34a) and (34b)]. Not going further than second-order time derivatives, for the sake of argument, we might maximize the entropy $\mathcal{S}_I$, using fixed values of $\langle E\rangle$, $\langle Z\rangle$,

$\langle dE/dt\rangle$, $\langle dZ/dt\rangle$, $\langle d^2E/dt^2\rangle$, and $\langle d^2Z/dt^2\rangle$ as constraints. The maximum entropy can then be written as

$$\mathcal{S}_M = \mathcal{S}_M\left(\langle E\rangle, \langle Z\rangle, \left\langle\frac{dE}{dt}\right\rangle, \left\langle\frac{dZ}{dt}\right\rangle, \left\langle\frac{d^2E}{dt^2}\right\rangle, \left\langle\frac{d^2Z}{dt^2}\right\rangle\right). \tag{79}$$

Note, however, that the actual expression might be different from (29) if the constraints are no longer of the form (14). Given that the last four arguments of $\mathcal{S}_M$ are fixed at the value zero, the entropy $\mathcal{S}_M$ is a function of $\langle E\rangle$ and $\langle Z\rangle$. The values of $\langle E\rangle$ and $\langle Z\rangle$ that maximize the entropy $\mathcal{S}_M$ can, as we have seen, be obtained by maximizing the entropy $\mathcal{S}_I$ with only these last four arguments as constraints. The resulting values of $\langle E\rangle$ and $\langle Z\rangle$ will now be different from the values obtained earlier—and possibly closer to the numerical values—as the constraints on the second-order time derivatives provide additional information. A theory developed along these lines would—for systems that have reached a state of statistical stationarity—be purely predictive because the only basic assumption is that the system's expected values $\langle E\rangle$ and $\langle Z\rangle$ do not change in time, so that $\langle dE/dt\rangle$, $\langle dZ/dt\rangle$, $\langle d^2E/dt^2\rangle$, $\langle d^2Z/dt^2\rangle$, etc., can be taken zero.[4]

It is not difficult to write out the constraints on the second-order time derivatives of E and Z, given above, and express them in terms of the spectral coefficients ψ_{mn} of the numerical model. If we do this, however, we will see that the Jacobian appears in the formulas so that the quantities contain terms of the form $\psi_{mn}\psi_{ij}$ and $\psi_{mn}\psi_{ij}\psi_{kl}$ with indices that may be different. On the one hand, these terms raise the prospect of obtaining correlations between different coefficients, correlations that are probably needed to reproduce the wavelike structures in the numerically averaged relative vorticity field. On the other hand, the same terms might cause problems in the calculation of the probability density function. It is also difficult to assess how far one has to go with the use of higher-order constraints. In principle, infinitely many of them could be used, although it is possible, of course, that the procedure would converge quickly so that we would need only a small number. These and similar issues are left as subjects of future research.

[4] The strategy proposed here is presumably an approximated application of the principle of maximum caliber to statistically stationary states (nonequilibrium steady states) that Jaynes (1980) has proposed as the guiding principle of nonequilibrium statistical mechanics.

Acknowledgments. The authors are grateful for support from the Lorentz Center, Leiden. They wish to thank Dr. Colm Connaughton for his contribution to the discussions at an early stage of this work. They also wish to express their gratitude to the reviewers for their constructive comments.

APPENDIX

Calculating the Lagrange Multipliers

In this appendix we give a few details on the way in which the Lagrange multipliers are calculated.

a. The unforced-undamped case

We first rewrite the expressions (56) for the variance and mean σ_{mn}^2 and μ_{mn}:

$$\sigma_{mn}^2 = \frac{1}{\beta}\frac{1}{\varepsilon_n(\alpha/\beta+\varepsilon_n)}, \quad \text{and} \quad \mu_{mn} = \frac{f_{mn}}{\alpha/\beta+\varepsilon_n}. \tag{A1}$$

This allows us to cast the expressions (57a) and (57b) of the expected energy and enstrophy in the following form:

$$\langle E\rangle - \sum_{mn}\frac{1}{2}\varepsilon_n\mu_{mn}^2 = \frac{1}{\beta}\sum_{mn}\frac{1}{2}\varepsilon_n s_{mn}^2 \quad \text{and} \tag{A2a}$$

$$\langle Z\rangle - \sum_{mn}\left(\frac{1}{2}\varepsilon_n^2\mu_{mn}^2 - \varepsilon_n f_{mn}\mu_{mn} + \frac{1}{2}f_{mn}^2\right) = \frac{1}{\beta}\sum_{mn}\frac{1}{2}\varepsilon_n^2 s_{mn}^2, \tag{A2b}$$

where we have defined

$$s_{mn}^2 = \frac{1}{\varepsilon_n(\alpha/\beta+\varepsilon_n)}. \tag{A3}$$

Because μ_{mn} and s_{mn} only depend on the fraction α/β, the quotient of the two equations above depends only on α/β. If we subtract the quotient on the right-hand side of the equality sign from the quotient on the left-hand side, the sought-for value of α/β is then a zero of the resulting expression. Plotting it as a function of α/β, the zero can be found by a simple numerical search algorithm. After α/β has been calculated to any degree of accuracy (e.g., by the method of interval halving), the value of β can be obtained by using any one of the two expressions above, from which α then immediately follows.

b. The forced-damped case

To find the Lagrange multipliers γ and δ in the case in which decay rates of energy and enstrophy are used as the sole constraints, a procedure is followed that is

closely analogous to the procedure described above. We first rewrite (67):

$$\sigma_{mn}^2 = \frac{1}{\delta}\frac{1}{2d_n(\gamma/\delta + \varepsilon_n)}, \quad \mu_{mn} = \frac{f_{mn}}{2(\gamma/\delta + \varepsilon_n)} - \frac{F_{mn}}{2d_{mn}}, \tag{A4}$$

which enables us to cast (68a) and (68b) in the form

$$\langle \mathcal{D} - \mathcal{F} \rangle - \sum_{mn}(d_n\mu_{mn}^2 + F_{mn}\mu_{mn}) = \frac{1}{\delta}\sum_{mn} d_n s_{mn}^2 \quad \text{and} \tag{A5a}$$

$$\langle \mathcal{H} - \mathcal{G} \rangle - \sum_{mn}[d_n\varepsilon_n\mu_{mn}^2 + (\varepsilon_n F_{mn} - d_n f_{mn}) - f_{mn}F_{mn}] = \frac{1}{\delta}\sum_{mn} d_n\varepsilon_n s_{mn}^2, \tag{A5b}$$

where we have defined

$$s_{mn}^2 = \frac{1}{2d_n(\gamma/\delta + \varepsilon_n)}. \tag{A6}$$

In exactly the same way as before, we may find γ/δ by dividing the second of the two equations by the first, subtracting the two quotients, and then searching for a zero of the resulting expression. Either one of the two original equations can then be used to find δ, from which γ follows.

In case we wish to use all four constraints (73) and (74), we rewrite (75) and (76):

$$\sigma_{mn}^2 = \frac{1}{\delta}\frac{1}{\varepsilon_n(\alpha/\delta + \beta/\delta\varepsilon_n) + 2d_n(\gamma/\delta + \varepsilon_n)} \quad \text{and} \tag{A7}$$

$$\mu_{mn} = \frac{(\beta/\delta\varepsilon_n + d_n)f_{mn} - (\gamma/\delta + \varepsilon_n)F_{mn}}{\varepsilon_n(\alpha/\delta + \beta/\delta\varepsilon_n) + 2d_n(\gamma/\delta + \varepsilon_n)}. \tag{A8}$$

We can then cast the different constraints in the form

$$\langle E \rangle - \sum_{mn}\frac{1}{2}\varepsilon_n\mu_{mn}^2 = \frac{1}{\delta}\sum_{mn}\frac{1}{2}\varepsilon_n s_{mn}^2, \tag{A9a}$$

$$\langle Z \rangle - \sum_{mn}\left(\frac{1}{2}\varepsilon_n^2\mu_{mn}^2 - \varepsilon_n f_{mn}\mu_{mn} + \frac{1}{2}f_{mn}^2\right) = \frac{1}{\delta}\sum_{mn}\frac{1}{2}\varepsilon_n^2 s_{mn}^2, \tag{A9b}$$

$$\langle \mathcal{D} - \mathcal{F} \rangle - \sum_{mn}(d_n\mu_{mn}^2 + F_{mn}\mu_{mn}) = \frac{1}{\delta}\sum_{mn} d_n s_{mn}^2 \quad \text{and} \tag{A9c}$$

$$\langle \mathcal{H} - \mathcal{G} \rangle - \sum_{mn}[d_n\varepsilon_n\mu_{mn}^2 + (\varepsilon_n F_{mn} - d_n f_{mn}) - f_{mn}F_{mn}] = \frac{1}{\delta}\sum_{mn} d_n\varepsilon_n s_{mn}^2, \tag{A9d}$$

where s_{mn}^2 is defined by

$$s_{mn}^2 = \frac{1}{\varepsilon_n(\alpha/\delta + \beta/\delta\,\varepsilon_n) + 2d_n(\gamma/\delta + \varepsilon_n)}. \tag{A10}$$

By dividing the second, third, and fourth of these equations by the first and then subtracting the right-hand sides from the left-hand sides, we may reduce the system to three equations in the three variables α/δ, β/δ, and γ/δ. From the solution of this system, δ can be obtained by using any one of the equations above, from which then α, β, and γ follow. The solution is sought graphically by plotting the zero lines of the second and third equations (obtained by the dividing procedure just described) as a function of α/δ and β/δ, where γ/δ is determined automatically by zero-searching of the third equation using interval halving. The values of α/δ and β/δ at which the two zero lines cross are the required values that, together with the automatically searched-for value of γ/δ, constitute the solution of the system. By zooming in successively, one may obtain values of α, β, γ, and δ to any required accuracy.

REFERENCES

Abramowitz, M., and I. Stegun, 1970: *Handbook of Mathematical Functions*. Dover, 1046 pp.

Ambaum, M., 1997: Isentropic formation of the tropopause. *J. Atmos. Sci.,* **54,** 555–568.

Batchelor, G. K., 1969: Computation of the energy spectrum in homogeneous two-dimensional turbulence. *Phys. Fluids,* (Suppl. II), **12,** 233–239.

Burgers, J. M., 1939: Mathematical examples illustrating relations occurring in the theory of turbulent fluid motion. *Proc. Roy. Neth. Acad. Sci. Amsterdam,* **17,** 1–53. [Reprinted in Nieuwstadt and Steketee (1995), 281–334.]

——, 1941: Beschouwingen over de statistische theorie der turbulente stroming. *Nederlands Tijdschrift voor Natuurkunde,* **8,** 5–18.

——, 1974: *The Nonlinear Diffusion Equation*. Reidel, 174 pp.

Carnevale, G. F., and J. S. Frederiksen, 1987: Nonlinear stability and statistical mechanics of flow over topography. *J. Fluid Mech.,* **175,** 157–181.

Charney, J. G., 1971: Geostrophic turbulence. *J. Atmos. Sci.,* **28,** 1087–1095.

Dritschel, D. G., C. V. Tran, and R. K. Scott, 2007: Revisiting Batchelor's theory of two-dimensional turbulence. *J. Fluid Mech.,* **591,** 379–391.

Eyink, G. L., and K. R. Sreenivasan, 2006: Onsager and the theory of hydrodynamic turbulence. *Rev. Mod. Phys.,* **78,** 87–135.

Frederiksen, J. S., and B. L. Sawford, 1981: Topographic waves in nonlinear and linear spherical barotropic models. *J. Atmos. Sci.,* **38,** 69–86.

Jaynes, E. T., 1957a: Information theory and statistical mechanics. *Phys. Rev.,* **106,** 620–630. [Reprinted in Rosenkrantz (1989), 4–16.]

——, 1957b: Information theory and statistical mechanics II. *Phys. Rev.,* **108,** 171–190. [Reprinted in Rosenkrantz (1989), 17–38.]

——, 1968: Prior probabilities. *IEEE Trans. Syst. Sci. Cybernetics,* **4,** 227–241. [Reprinted in Rosenkrantz (1989), 114–130.]

——, 1973: The well-posed problem. *Found. Phys.,* **3,** 477–493. [Reprinted in Rosenkrantz (1989), 131–148.]

——, 1980: The minimum entropy production principle. *Annu. Rev. Phys. Chem.,* **31,** 579–601. [Reprinted in Rosenkrantz (1989), 401–424.]

Kraichnan, R. H., 1967: Inertial ranges in two-dimensional turbulence. *Phys. Fluids,* **10,** 1417–1423.

——, and D. Montgomery, 1980: Two-dimensional turbulence. *Rep. Prog. Phys.,* **43,** 547–619.

Kurgansky, M. V., 2008: The energy spectrum in a barotropic atmosphere. *Adv. Geosci.,* **15,** 17–22.

Machenhauer, B., 1979: The spectral method. *Numerical Methods Used in Atmospheric Models,* Vol. II, WMO/GARP Publ. Ser. 17, 121–275.

Majda, A. J., and X. Wang, 2006: *Nonlinear Dynamics and Statistical Theories for Basic Geophysical Flows*. Cambridge University Press, 551 pp.

McWilliams, J. C., 1984: The emergence of isolated coherent vortices in turbulent flow. *J. Fluid Mech.,* **146,** 21–43.

Miller, J., 1990: Statistical mechanics of Euler equations in two dimensions. *Phys. Rev. Lett.,* **65,** 2137–2140.

——, P. B. Weichman, and M. C. Cross, 1992: Statistical mechanics, Euler's equation and Jupiter's Red Spot. *Phys. Rev.,* **45A,** 2328–2359.

Nieuwstadt, F. T. M., and J. A. Steketee, Eds., 1995: *Selected Papers of J. M. Burgers*. Kluwer Academic, 650 pp.

Onsager, L., 1949: Statistical hydrodynamics. *Nuovo Cimento,* **6,** 279–287.

Pasmanter, R. A., 1994: On long-lived vortices in 2-D viscous flows, most probable states of inviscid 2-D flows and a soliton equation. *Phys. Fluids,* **6,** 1236–1241.

Peixoto, J. P., and A. H. Oort, 1992: *Physics of Climate*. American Institute of Physics, 520 pp.

Robert, R., and J. Sommeria, 1991: Statistical equilibrium states for two-dimensional flows. *J. Fluid Mech.,* **229,** 291–310.

——, and ——, 1992: Relaxation towards a statistical equilibrium state in two-dimensional perfect fluid dynamics. *Phys. Rev. Lett.,* **69,** 2776–2779.

Rosenkrantz, R. D., Ed., 1989: *E. T. Jaynes: Papers on Probability, Statistics and Statistical Physics*. Kluwer Academic, 434 pp.

Salmon, R., 1998: *Lectures on Geophysical Fluid Dynamics*. Oxford University Press, 378 pp.

Schubert, W. H., R. K. Taft, and L. G. Silvers, 2009: Shallow water quasi-geostrophic theory on the sphere. *J. Adv. Model. Earth Syst.,* in press [Available online at http://adv-model-earth-syst.org/index.php/JAMES/article/view/1.]

Thompson, P. D., 1973: The equilibrium energy spectrum of randomly forced two-dimensional turbulence. *J. Atmos. Sci.,* **30,** 1593–1598.

Verkley, W. T. M., 2009: A balanced approximation of the one-layer shallow-water equations on a sphere. *J. Atmos. Sci.,* **66,** 1735–1748.